Comput. Methods Appl. Mech. Engrg. 198 (2009) 1609–1630

Contents lists available at ScienceDirect

Comput. Methods Appl. Mech. Engrg.

journal homepage: www.elsevier.com/locate/cma

On the use of geometrically exact shells in a conserving framework for flexible multibody dynamics

Peter Betsch *, Nicolas Sänger

Chair of Computational Mechanics, Department of Mechanical Engineering, University of Siegen, Paul-Bonatz-Str. 9-11, 57068 Siegen, Germany

ARTICLE INFO

Article history:
Received 19 November 2008
Received in revised form 13 January 2009
Accepted 20 January 2009
Available online 29 January 2009

Keywords:
Shell finite elements
Multibody dynamics
Finite rotations
Energy–momentum schemes

ABSTRACT

The present work deals with the design of energy–momentum conserving schemes for flexible multibody dynamics. The proposed approach is based on nonlinear finite element methods for the space discretization of flexible bodies. In particular, the focus is on geometrically exact shells relying on Reissner–Mindlin kinematics. It is shown that the equations of motion pertaining to the semi-discrete shell formulation can be written in the form of differential-algebraic equations (DAEs). The DAEs provide a uniform framework for a rotationless description of flexible multibody dynamics. The use of rotational parameters is circumvented throughout the discretization process in space and time. The rotationless description facilitates the straightforward incorporation of geometrically exact shells (and beams) into a multibody framework. In addition to that, the advocated approach makes possible the design of a uniform energy–momentum conserving time-stepping scheme for general multibody systems. Numerical examples demonstrate the excellent numerical stability properties of the present scheme. Moreover, comparison is made with more traditional formulations based on rotational parameters.

1. Introduction

The present work deals with the incorporation of flexible shell structures into multibody systems. In particular, we focus on the discretization in space and time of geometrically exact shells relying on classical Reissner–Mindlin kinematics. Our approach makes possible a uniform computational treatment of nonlinear shells and flexible multibody systems.

In the last years the extension of finite element methods for rigid bodies has been treated by Puso [34] and Göttlicher and Schweizerhof [23]. Nonlinear beam finite elements have been incorporated into multibody dynamics, for example, by Bauchau and Bottasso [2], Ibrahimbegović et al. [26], Bottasso et al. [14], Jelenić and Crisfield [27], Taylor [42], Betsch and Steinmann [9] and Muñoz and Jelenić [33]. Only few works deal with nonlinear shell finite elements in the context of multibody dynamics, see Bauchau et al. [3].

The first energy–momentum conserving (EM) scheme for geo-

mo and Tarnow

lementation. En-

Géradin and Cardona [20] for a summary of previous developments until the turn of the millennium.

Main ingredients of contemporary finite element methods for nonlinear structural dynamics are (i) geometrically exact formulations which rely on nonlinear strain measures and can cope with both finite strains and arbitrarily large rigid body motions, and (ii) energy–momentum conserving schemes (or energy decaying variants thereof) which make possible the stable time integration of the stiff[1] nonlinear ODEs resulting from the space discretization.

It was realized soon that these methods possess great potential for the computer simulation of flexible multibody dynamics. For example, the coupling of nonlinear continuum elements to

ergy decaying variants of the EM scheme have been proposed by Bottasso et al. [13] and Romero and Armero [35]. The Newmark-type scheme developed by Simo et al. [38] can be regarded as precursor of the EM scheme. The Newmark-type scheme conserves angular momentum and has been extended to the realm of geometrically exact sandwich shells by Vu-Quoc et al. [28]. Alternative Newmark-type schemes on the rotation manifold have been developed in the context of nonlinear shells by Lubowiecka and Chróścielewski [31] and Brank et al. [16].

In nonlinear structural dynamics, the semi-discrete equations of motion resulting from the finite element discretization in space are commonly treated as ODEs on the rotation manifold. Accordingly, rotational parameters are an integral part of the time discretization. In contrast to that, in the present work we regard the ODEs on the rotation manifold as differential-algebraic equations (DAEs). This viewpoint turns out to be especially beneficial to (i) the incorporation of geometrically exact shells (and beams)

* Corresponding author.
E-mail address: betsch@imr.mb.uni-siegen.de (P. Betsch).

[1] In the case of shells the stiffness is typically dominated by the material contributions associated with the membrane and transverse shear strains.

0045-7825
doi:10.1016/j.cma.2009.01.016

into multibody systems, and (ii) the design of EM schemes for flexible multibody dynamics in general.

We present the first EM scheme for multibody systems containing geometrically exact shells. Moreover, we compare our rotationless discretization approach with previous approaches relying on rotational parameters. We show that the advocated uniform algorithmic treatment of displacements and rotations has several advantages over the traditional use of rotational parameters.

An outline of the rest of the paper is as follows: Section 2 provides a summary of the main ingredients of the geometrically exact shell model needed for the subsequent discretization process. The discretization in space is treated in Section 3, while the discretization in time is dealt with in Section 4. Details of the present algorithmic treatment of finite rotations are presented within a suitable model problem in Section 5. Moreover, in Section 5, the advocated rotationless discretization approach is compared with more common methods relying on rotational parameters. The incorporation of shells into multibody systems is presented in Section 6. Several numerical examples dealing with the dynamics of shells and flexible multibody systems are dealt with in Section 7. Eventually, conclusions are drawn.

2. Summary of the shell formulation

The present work aims at nonlinear shell formulations relying on classical Reissner–Mindlin kinematics. In particular, we start from the stress resultant geometrically exact shell model described in Simo and Fox [37]. The nonlinear shell formulation belongs to the class of special Cosserat shells, see Antman [1, Chapter 17]. However, in essence, the present approach can be directly applied to any degenerate continuum (or continuum-based) C^0 shell element.

This section provides a summary of the variational shell equations which form the basis of the finite element discretization in space. Additionally, we outline important conservation properties of the continuous shell formulation which shall be conserved under discretization.

Let $\boldsymbol{s}=(s^1,s^2)\in\mathscr{A}\subset\mathbb{R}^2$ be curvilinear coordinates for the mid-surface $\mathscr{S}$ of the shell. Then the map $\boldsymbol{\varphi}:\mathscr{A}\mapsto\mathbb{R}^3$ defines the position of material points on the mid-surface $\mathscr{S}$. In addition to that, the director field $\boldsymbol{d}:\mathscr{A}\mapsto\mathsf{S}^2\subset\mathbb{R}^3$ characterizes the orientation of material fibers normal to the mid-surface $\mathscr{S}^0$ in the reference configuration. In this connection, the unit sphere in $\mathbb{R}^3$ is defined by

$$\mathsf{S}^2=\{\boldsymbol{d}\in\mathbb{R}^3\,|\,\|\boldsymbol{d}\|=1\}. \tag{1}$$

Accordingly, the configuration space of the shell is given by

$$\mathsf{Q}=\left\{\boldsymbol{\Phi}=(\boldsymbol{\varphi},\boldsymbol{d}):\mathscr{A}\mapsto\mathbb{R}^3\times\mathsf{S}^2\,|\,\boldsymbol{\varphi}|_{\partial\mathscr{S}_\varphi}=\bar{\boldsymbol{\varphi}}\text{ and }\boldsymbol{d}|_{\partial\mathscr{S}_d}=\bar{\boldsymbol{d}}\right\}, \tag{2}$$

where $\bar{\boldsymbol{\varphi}}$ and $\bar{\boldsymbol{d}}$ are prescribed at different parts of the boundary $\partial\mathscr{S}$. The space of test functions coincides with the tangent space to Q given by

$$\mathsf{V}=\left\{\delta\boldsymbol{\Phi}=(\delta\boldsymbol{\varphi},\delta\boldsymbol{d}):\mathscr{A}\mapsto\mathbb{R}^3\times T_d\mathsf{S}^2|\delta\boldsymbol{\varphi}|_{\partial\mathscr{S}_\varphi}=\boldsymbol{0}\text{ and }\delta\boldsymbol{d}|_{\partial\mathscr{S}_d}=\boldsymbol{0}\right\}. \tag{3}$$

Here, $T_d\mathsf{S}^2$ denotes the tangent space to the unit sphere at $\boldsymbol{d}\in\mathsf{S}^2$ defined by

$$T_d\mathsf{S}^2=\{\delta\boldsymbol{d}\in\mathbb{R}^3|\boldsymbol{d}\cdot\delta\boldsymbol{d}=0\}. \tag{4}$$

The weak form of the momentum balance equations pertaining to the geometrically exact shell formulation can be written in the form

$$G(\boldsymbol{\Phi};\delta\boldsymbol{\Phi})=G_{\text{dyn}}(\boldsymbol{\Phi};\delta\boldsymbol{\Phi})+G_{\text{int}}(\boldsymbol{\Phi};\delta\boldsymbol{\Phi})-G_{\text{ext}}(\delta\boldsymbol{\Phi})=0, \tag{5}$$

where G_{ext} can be interpreted as virtual work of the external loading and G_{dyn} is the contribution of the inertia terms defined by

$$G_{\text{dyn}}(\boldsymbol{\Phi};\delta\boldsymbol{\Phi})=\int_{\mathscr{S}^0}[A_{\varrho_0}\delta\boldsymbol{\varphi}\cdot\ddot{\boldsymbol{\varphi}}+I_{\varrho_0}\delta\boldsymbol{d}\cdot\ddot{\boldsymbol{d}}]\,\mathrm{d}\mathscr{S}. \tag{6}$$

Here, A_{ϱ_0} is the (time-independent) nominal surface density and I_{ϱ_0} is the (time-independent) nominal rotational inertia of the shell. Furthermore, G_{int} is the virtual work of the internal forces given by the following expression:

$$G_{\text{int}}(\boldsymbol{\Phi};\delta\boldsymbol{\Phi})=\int_{\mathscr{S}^0}\left[\frac{\partial\widehat{W}}{\partial\boldsymbol{\varphi}_{,\alpha}}\cdot\delta\boldsymbol{\varphi}_{,\alpha}+\frac{\partial\widehat{W}}{\partial\boldsymbol{d}_{,\alpha}}\cdot\delta\boldsymbol{d}_{,\alpha}+\frac{\partial\widehat{W}}{\partial\boldsymbol{d}}\cdot\delta\boldsymbol{d}\right]\mathrm{d}\mathscr{S}. \tag{7}$$

The stored energy function $W=\widehat{W}(\boldsymbol{\varphi}_{,\alpha},\boldsymbol{d}_{,\alpha},\boldsymbol{d})$ accounts for hyperelastic material behavior and assumes the specific form

$$W=\widetilde{W}(a_{\alpha\beta},\kappa_{\alpha\beta},\gamma_\alpha) \tag{8}$$

with the set of kinematic quantities

$$a_{\alpha\beta}=\boldsymbol{\varphi}_{,\alpha}\cdot\boldsymbol{\varphi}_{,\beta};\quad\kappa_{\alpha\beta}=\boldsymbol{\varphi}_{,\alpha}\cdot\boldsymbol{d}_{,\beta}+\boldsymbol{d}_{,\alpha}\cdot\boldsymbol{\varphi}_{,\beta};\quad\gamma_\alpha=\boldsymbol{\varphi}_{,\alpha}\cdot\boldsymbol{d}. \tag{9}$$

Note that (8) implies that the constitutive equations are invariant under rigid motions which conforms with the fundamental principle of frame-indifference. Let $\boldsymbol{\Phi}^\sharp=(\boldsymbol{\varphi}^\sharp,\boldsymbol{d}^\sharp)\in\mathsf{Q}$ define a motion that differs from $\boldsymbol{\Phi}=(\boldsymbol{\varphi},\boldsymbol{d})\in\mathsf{Q}$ by a rigid motion. Then there is a vector $\boldsymbol{c}(t)\in\mathbb{R}^3$ and a rotation tensor $\boldsymbol{Q}(t)\in\mathsf{SO}(3)$ such that

$$\begin{aligned}\boldsymbol{\varphi}^\sharp(\boldsymbol{s},t)&=\boldsymbol{c}(t)+\boldsymbol{Q}(t)\boldsymbol{\varphi}(\boldsymbol{s},t),\\ \boldsymbol{d}^\sharp(\boldsymbol{s},t)&=\boldsymbol{Q}(t)\boldsymbol{d}(\boldsymbol{s},t).\end{aligned} \tag{10}$$

It can be easily verified that the kinematic quantities in (9) are invariant under rigid motions. For example,

$$a^\sharp_{\alpha\beta}=\boldsymbol{\varphi}^\sharp_{,\alpha}\cdot\boldsymbol{\varphi}^\sharp_{,\beta}=\boldsymbol{\varphi}_{,\alpha}\cdot\boldsymbol{Q}^T\boldsymbol{Q}\boldsymbol{\varphi}_{,\beta}=\boldsymbol{\varphi}_{,\alpha}\cdot\boldsymbol{\varphi}_{,\beta}=a_{\alpha\beta}. \tag{11}$$

Similarly, $\kappa^\sharp_{\alpha\beta}=\kappa_{\alpha\beta}$ and $\gamma^\sharp_\alpha=\gamma_\alpha$, so that $\widetilde{W}(a^\sharp_{\alpha\beta},\kappa^\sharp_{\alpha\beta},\gamma^\sharp_\alpha)=\widetilde{W}(a_{\alpha\beta},\kappa_{\alpha\beta},\gamma_\alpha)$. Alternatively, rotational invariance of the stored energy function implies that

$$\widehat{W}(\boldsymbol{Q}\boldsymbol{\varphi}_{,\alpha},\boldsymbol{Q}\boldsymbol{d}_{,\alpha},\boldsymbol{Q}\boldsymbol{d})=\widehat{W}(\boldsymbol{\varphi}_{,\alpha},\boldsymbol{d}_{,\alpha},\boldsymbol{d}). \tag{12}$$

Let $\boldsymbol{Q}_\varepsilon=\exp_{\mathsf{SO}(3)}(\varepsilon\widehat{\boldsymbol{\xi}})\in\mathsf{SO}(3)$ for any $\varepsilon\in\mathbb{R}$ and skew-symmetric tensor $\widehat{\boldsymbol{\xi}}\in\mathsf{so}(3)$. In this connection, $\exp_{\mathsf{SO}(3)}$ denotes the exponential map on the rotation group, see Section 5.1 for further details. Rotational invariance of the stored energy function yields

$$\begin{aligned}0&=\left.\frac{\mathrm{d}}{\mathrm{d}\varepsilon}\right|_{\varepsilon=0}\widehat{W}(\boldsymbol{Q}_\varepsilon\boldsymbol{\varphi}_{,\alpha},\boldsymbol{Q}_\varepsilon\boldsymbol{d}_{,\alpha},\boldsymbol{Q}_\varepsilon\boldsymbol{d})\\&=\frac{\partial\widehat{W}}{\partial\boldsymbol{\varphi}_{,\alpha}}\cdot\widehat{\boldsymbol{\xi}}\boldsymbol{\varphi}_{,\alpha}+\frac{\partial\widehat{W}}{\partial\boldsymbol{d}_{,\alpha}}\cdot\widehat{\boldsymbol{\xi}}\boldsymbol{d}_{,\alpha}+\frac{\partial\widehat{W}}{\partial\boldsymbol{d}}\cdot\widehat{\boldsymbol{\xi}}\boldsymbol{d}\\&=-\boldsymbol{\xi}\cdot\left[\frac{\partial\widehat{W}}{\partial\boldsymbol{\varphi}_{,\alpha}}\times\boldsymbol{\varphi}_{,\alpha}+\frac{\partial\widehat{W}}{\partial\boldsymbol{d}_{,\alpha}}\times\boldsymbol{d}_{,\alpha}+\frac{\partial\widehat{W}}{\partial\boldsymbol{d}}\times\boldsymbol{d}\right]\end{aligned} \tag{13}$$

for any $\boldsymbol{\xi}\in\mathbb{R}^3$.

2.1. Conservation properties

We next outline important conservation laws which shall be preserved under discretization. Our exposition serves the additional purpose of introducing further shell-specific quantities required in the sequel.

2.1.1. Total linear momentum

The total linear momentum of the shell is defined by

$$\boldsymbol{L}=\int_{\mathscr{S}^0}A_{\varrho_0}\dot{\boldsymbol{\varphi}}\,\mathrm{d}\mathscr{S}. \tag{14}$$

In the case of vanishing external loading (i.e. $G_{\text{ext}}=0$) and pure Neumann boundary conditions the total linear momentum is a conserved quantity. To see this, choose specific test functions of the form $\delta\boldsymbol{\Phi}=(\delta\boldsymbol{\varphi},\delta\boldsymbol{d})=(\boldsymbol{\xi},\boldsymbol{0})$, where $\boldsymbol{\xi}\in\mathbb{R}^3$ is constant and arbitrary.

In view of (7), $G_{\rm int}(\boldsymbol{\Phi};(\xi,\boldsymbol{0}))=0$. In addition to that, with regard to (6), $G_{\rm dyn}(\boldsymbol{\Phi};(\xi,\boldsymbol{0}))=\xi\cdot\int_{\mathscr{S}^0}A_{\varrho_0}\ddot{\boldsymbol{\varphi}}\,\mathrm{d}\mathscr{S}$. Accordingly, the weak form (5) yields

$$G(\boldsymbol{\Phi};(\xi,\boldsymbol{0}))=\xi\cdot\dot{\boldsymbol{L}}=0. \tag{15}$$

Consequently, $\boldsymbol{L}$ is an integral of the motion.

2.1.2. Total angular momentum

The total angular momentum of the shell is defined by

$$\boldsymbol{J}=\int_{\mathscr{S}^0}[A_{\varrho_0}\boldsymbol{\varphi}\times\dot{\boldsymbol{\varphi}}+I_{\varrho_0}\boldsymbol{d}\times\dot{\boldsymbol{d}}]\,\mathrm{d}\mathscr{S}. \tag{16}$$

Consider the case of pure Neumann boundary conditions along with test functions of the form $\delta\boldsymbol{\Phi}=(\delta\boldsymbol{\varphi},\delta\boldsymbol{d})=(\xi\times\boldsymbol{\varphi},\xi\times\boldsymbol{d})$, where $\xi\in\mathbb{R}^3$ is constant. Under the assumption that $G_{\rm ext}(\boldsymbol{\Phi};(\xi\times\boldsymbol{\varphi},\xi\times\boldsymbol{d}))=0$, the momentum map $J_\xi=\boldsymbol{J}\cdot\xi$ is a constant of the motion. This property is a consequence of the rotational invariance of the stored energy function. Accordingly, with regard to (7),

$$\begin{aligned}&G_{\rm int}(\boldsymbol{\Phi};(\xi\times\boldsymbol{\varphi},\xi\times\boldsymbol{d}))\\&=\int_{\mathscr{S}^0}\left[\frac{\partial\widehat{W}}{\partial\boldsymbol{\varphi}_{,\alpha}}\cdot(\xi\times\boldsymbol{\varphi}_{,\alpha})+\frac{\partial\widehat{W}}{\partial\boldsymbol{d}_{,\alpha}}\cdot(\xi\times\boldsymbol{d}_{,\alpha})+\frac{\partial\widehat{W}}{\partial\boldsymbol{d}}\cdot(\xi\times\boldsymbol{d})\right]\mathrm{d}\mathscr{S}\\&=-\xi\cdot\int_{\mathscr{S}^0}\left[\frac{\partial\widehat{W}}{\partial\boldsymbol{\varphi}_{,\alpha}}\times\boldsymbol{\varphi}_{,\alpha}+\frac{\partial\widehat{W}}{\partial\boldsymbol{d}_{,\alpha}}\times\boldsymbol{d}_{,\alpha}+\frac{\partial\widehat{W}}{\partial\boldsymbol{d}}\times\boldsymbol{d}\right]\mathrm{d}\mathscr{S}=0,\end{aligned} \tag{17}$$

where use has been made of (13). In addition to that, (6) yields

$$\begin{aligned}G_{\rm dyn}(\boldsymbol{\Phi};(\xi\times\boldsymbol{\varphi},\xi\times\boldsymbol{d}))&=\xi\cdot\int_{\mathscr{S}^0}[A_{\varrho_0}\boldsymbol{\varphi}\times\ddot{\boldsymbol{\varphi}}+I_{\varrho_0}\boldsymbol{d}\times\ddot{\boldsymbol{d}}]\,\mathrm{d}\mathscr{S}\\&=\xi\cdot\frac{\mathrm{d}}{\mathrm{d}t}\int_{\mathscr{S}^0}[A_{\varrho_0}\boldsymbol{\varphi}\times\dot{\boldsymbol{\varphi}}+I_{\varrho_0}\boldsymbol{d}\times\dot{\boldsymbol{d}}]\,\mathrm{d}\mathscr{S}.\end{aligned} \tag{18}$$

To summarize, the weak form (5) yields

$$G(\boldsymbol{\Phi};(\xi\times\boldsymbol{\varphi},\xi\times\boldsymbol{d}))=\xi\cdot\dot{\boldsymbol{J}}=\frac{\mathrm{d}}{\mathrm{d}t}J_\xi=0 \tag{19}$$

so that J_ξ is conserved.

2.1.3. Total energy

If the external loads can be derived from a potential energy functional $V_{\rm ext}(\boldsymbol{\Phi})$, which does not depend explicitly on time, the mechanical system under consideration can be identified as autonomous Hamiltonian system. Conservation of the Hamiltonian (or the total energy) can be easily verified by inserting $\delta\boldsymbol{\Phi}=(\delta\boldsymbol{\varphi},\delta\boldsymbol{d})=(\dot{\boldsymbol{\varphi}},\dot{\boldsymbol{d}})$ into the weak form (5). Accordingly, (7) gives

$$G_{\rm int}(\boldsymbol{\Phi};(\dot{\boldsymbol{\varphi}},\dot{\boldsymbol{d}}))=\frac{\mathrm{d}}{\mathrm{d}t}\int_{\mathscr{S}^0}\widehat{W}(\boldsymbol{\varphi}_{,\alpha},\boldsymbol{d}_{,\alpha},\boldsymbol{d})\,\mathrm{d}\mathscr{S}. \tag{20}$$

Introducing the total potential

$$V(\boldsymbol{\Phi})=V_{\rm int}(\boldsymbol{\Phi})+V_{\rm ext}(\boldsymbol{\Phi}) \tag{21}$$

with

$$V_{\rm int}(\boldsymbol{\Phi})=\int_{\mathscr{S}^0}\widehat{W}(\boldsymbol{\varphi}_{,\alpha},\boldsymbol{d}_{,\alpha},\boldsymbol{d})\,\mathrm{d}\mathscr{S}, \tag{22}$$

we may write

$$G_{\rm int}(\boldsymbol{\Phi};(\dot{\boldsymbol{\varphi}},\dot{\boldsymbol{d}}))-G_{\rm ext}((\dot{\boldsymbol{\varphi}},\dot{\boldsymbol{d}}))=\frac{\mathrm{d}}{\mathrm{d}t}[V_{\rm int}+V_{\rm ext}]=\frac{dV}{dt}. \tag{23}$$

Moreover, introducing the kinetic energy

$$T=\frac{1}{2}\int_{\mathscr{S}^0}[A_{\varrho_0}\|\dot{\boldsymbol{\varphi}}\|^2+I_{\varrho_0}\|\dot{\boldsymbol{d}}\|^2]\,\mathrm{d}\mathscr{S} \tag{24}$$

expression (6) for the contribution to the weak form of the inertial terms yields

$$G_{\rm dyn}(\boldsymbol{\Phi};(\dot{\boldsymbol{\varphi}},\dot{\boldsymbol{d}}))=\int_{\mathscr{S}^0}[A_{\varrho_0}\dot{\boldsymbol{\varphi}}\cdot\ddot{\boldsymbol{\varphi}}+I_{\varrho_0}\dot{\boldsymbol{d}}\cdot\ddot{\boldsymbol{d}}]\,\mathrm{d}\mathscr{S}=\frac{dT}{dt}. \tag{25}$$

To summarize, the weak form (5) yields

$$G(\boldsymbol{\Phi};(\dot{\boldsymbol{\varphi}},\dot{\boldsymbol{d}}))=\frac{\mathrm{d}}{\mathrm{d}t}[T+V]=0. \tag{26}$$

Thus the total energy $T+V$ is an integral of the motion.

3. Semi-discrete shell formulation

We next deal with the Galerkin finite element approximation of the weak form (5). For the discretization in space of a configuration $\boldsymbol{\Phi}=(\boldsymbol{\varphi},\boldsymbol{d})\in\mathrm{Q}$ we make use of standard isoparametric interpolations of the form Fig. 1

$$\boldsymbol{\Phi}^h(\boldsymbol{s})=\sum_{A=1}^{n_{node}}N^A(\boldsymbol{s})\boldsymbol{q}_A. \tag{27}$$

Here $N^A(\boldsymbol{s})$, $A=1,\ldots,n_{node}$, are Lagrangian shape functions with associated nodal values (see Fig. 2)

$$\boldsymbol{q}_A=(\boldsymbol{\varphi}_A,\boldsymbol{d}_A)\in\mathbb{R}^3\times\mathrm{S}^2. \tag{28}$$

Note that the present finite element approximation relies on the nodal interpolation of the director field $\boldsymbol{d}\in\mathrm{S}^2$. It is worth mentioning that the director interpolation is a characteristic feature of degenerate shell elements (cf. Büchter and Ramm [17]). Moreover, it has been shown in Simo et al. [38], that the director interpolation is a prerequisite for maintaining conservation of angular momentum in the semi-discrete shell formulation.

Interpolation (27) entails that both the essential boundary conditions as well as the unit-length condition on the director field are confined to the nodal points. Accordingly, in the semi-discrete shell formulation, both conditions can be written as algebraic constraints on the nodal values. Typically, the constraints due to the essential boundary conditions can be cast in the form

$$\boldsymbol{G}_{\rm ext}\boldsymbol{q}=\boldsymbol{b}, \tag{29}$$

where $\boldsymbol{b}$ contains prescribed values associated with the Dirichlet boundary conditions and $\boldsymbol{q}\in\mathbb{R}^{6n_{\rm node}}$ is the nodal configuration vector of the semi-discrete shell given by

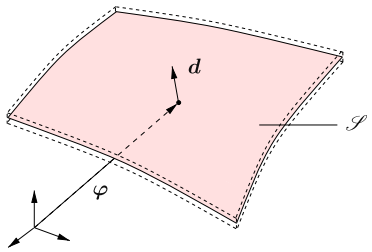

Fig. 1. The free shell described in terms of $(\boldsymbol{\varphi},\boldsymbol{d})\in\mathbb{R}^3\times\mathrm{S}^2$.

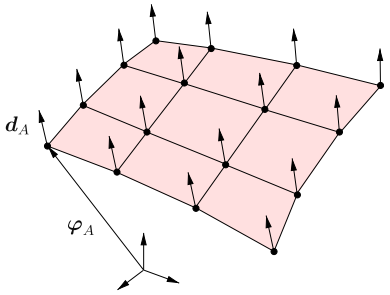

Fig. 2. The free semi-discrete shell with nodal coordinates $(\boldsymbol{\varphi}_A,\boldsymbol{d}_A)\in\mathbb{R}^3\times\mathrm{S}^2$.

$$\boldsymbol{q}=\begin{bmatrix}\boldsymbol{q}_1\\ \boldsymbol{q}_2\\ \vdots\\ \boldsymbol{q}_{n_{\text{node}}}\end{bmatrix}. \tag{30}$$

In addition to the 'external' constraints associated with the Dirichlet boundary conditions there are n_{node} 'internal' constraints related to the inextensibility condition on the nodal directors. Accordingly, the nodal configuration space is given by

$$\mathrm{Q}_{\text{node}}=\left\{\boldsymbol{q}\in\mathbb{R}^{6n_{\text{node}}}|\boldsymbol{G}_{\text{ext}}\boldsymbol{q}=\boldsymbol{b},\ \frac{1}{2}(\|\boldsymbol{d}_A\|^2-1)=0,\ A=1,2,\dots,n_{\text{node}}\right\}. \tag{31}$$

The finite element approximation of the configuration space can now be written as

$$\mathrm{Q}^h=\left\{\boldsymbol{\Phi}^h=(\boldsymbol{\varphi}^h,\boldsymbol{d}^h)|\boldsymbol{\Phi}^h=\sum_{A=1}^{n_{\text{node}}}N^A\boldsymbol{q}_A,\boldsymbol{q}\in\mathrm{Q}_{\text{node}}\right\}. \tag{32}$$

Similarly, the finite element approximation of the test functions yields

$$\mathrm{V}^h=\left\{\delta\boldsymbol{\Phi}^h=(\delta\boldsymbol{\varphi}^h,\delta\boldsymbol{d}^h)|\delta\boldsymbol{\Phi}^h=\sum_{A=1}^{n_{\text{node}}}N^A\delta\boldsymbol{q}_A,\ \ \delta\boldsymbol{q}\in T_q\mathrm{Q}_{\text{node}}\right\} \tag{33}$$

with the nodal tangent space at $\boldsymbol{q}\in\mathrm{Q}_{\text{node}}$ given by

$$T_q\mathrm{Q}_{\text{node}}=\left\{\delta\boldsymbol{q}\in\mathbb{R}^{6n_{\text{node}}}|\boldsymbol{G}_{\text{ext}}\delta\boldsymbol{q}=\boldsymbol{0},\ \boldsymbol{d}_A\cdot\delta\boldsymbol{d}_A=0,\ A=1,2,\dots,n_{\text{node}}\right\}. \tag{34}$$

The nonlinear constraints on the nodal directors are commonly accounted for by introducing two rotational parameters for S^2, leading to a total of five degrees of freedom per node, see, for example, Belytschko et al. [4, Chapter 9]. In the present work, we refrain from introducing rotational parameters at this stage and rather keep the redundant coordinates subject to algebraic constraints. This viewpoint will turn out to be beneficial to (i) the incorporation of shells into multibody systems, and (ii) the design of conserving time stepping schemes.

Incorporating the finite element approximations into the weak form (5) leads to the following semi-discrete shell problem: find $\boldsymbol{\Phi}^h\in\mathrm{Q}^h$ such that for all $\delta\boldsymbol{\Phi}^h\in\mathrm{V}^h$:

$$G(\boldsymbol{\Phi}^h,\delta\boldsymbol{\Phi}^h)=0. \tag{35}$$

We next provide alternative, more explicit, representations of the finite-dimensional shell problem at hand. With regard to (5), the last equation can be rewritten in the form

$$\sum_{A,B=1}^{n_{\text{node}}}\delta\boldsymbol{q}_A\cdot\boldsymbol{M}^{AB}\ddot{\boldsymbol{q}}_B+G_{\text{int}}(\boldsymbol{\Phi}^h,\delta\boldsymbol{\Phi}^h)-G_{\text{ext}}(\delta\boldsymbol{\Phi}^h)=0, \tag{36}$$

where $\boldsymbol{M}^{AB}$ are 6×6 nodal sub-matrices of the consistent mass matrix given by

$$\boldsymbol{M}^{AB}=\begin{bmatrix}M_\varphi^{AB}\boldsymbol{I}&\boldsymbol{0}\\ \boldsymbol{0}&M_d^{AB}\boldsymbol{I}\end{bmatrix}\quad\text{with}\quad\begin{aligned}M_\varphi^{AB}&=\int_{\mathscr{S}^0}A_\varrho N^AN^B\,\mathrm{d}\mathscr{S},\\ M_d^{AB}&=\int_{\mathscr{S}^0}I_\varrho N^AN^B\,\mathrm{d}\mathscr{S}.\end{aligned} \tag{37}$$

Inserting the finite element interpolations (27) into expression (21) for the potential energy yields the discrete function $V^h(\boldsymbol{q})=V(\boldsymbol{\Phi}^h)$, or

$$V^h(\boldsymbol{q})=V^h_{\text{int}}(\boldsymbol{q})+V^h_{\text{ext}}(\boldsymbol{q}). \tag{38}$$

Moreover, similar to (23), we get

$$\begin{aligned}G_{\text{int}}(\boldsymbol{\Phi}^h,\delta\boldsymbol{\Phi}^h)-G_{\text{ext}}(\delta\boldsymbol{\Phi}^h)&=\left[\nabla V^h_{\text{int}}(\boldsymbol{q})+\nabla V^h_{\text{ext}}(\boldsymbol{q})\right]\cdot\delta\boldsymbol{q}\\ &=\sum_{A=1}^{n_{\text{node}}}\left[\boldsymbol{F}^A_{\text{int}}(\boldsymbol{q})-\boldsymbol{F}^A_{\text{ext}}(t)\right]\cdot\delta\boldsymbol{q}_A,\end{aligned} \tag{39}$$

where the internal and external nodal forces, $\boldsymbol{F}^A_{\text{int}}$ and $\boldsymbol{F}^A_{\text{ext}}$, respectively, have been introduced. Concerning the internal nodal forces a straightforward calculation yields

$$\boldsymbol{F}^A_{\text{int}}=\begin{bmatrix}\int_{\mathscr{S}^0}\left[2\frac{\widetilde{\partial W}}{\partial\kappa_{\alpha\beta}}\boldsymbol{\varphi}^h_{,\alpha}+2\frac{\widetilde{\partial W}}{\partial\kappa_{\alpha\beta}}\boldsymbol{d}^h_{,\alpha}+\frac{\widetilde{\partial W}}{\partial\gamma_\beta}\boldsymbol{d}^h\right]N^A_{,\beta}\,\mathrm{d}\mathscr{S}\\ \int_{\mathscr{S}^0}\left[2\frac{\widetilde{\partial W}}{\partial\kappa_{\alpha\beta}}N^A_{,\beta}+\frac{\widetilde{\partial W}}{\partial\gamma_\alpha}N^A\right]\boldsymbol{\varphi}^h_{,\alpha}\,\mathrm{d}\mathscr{S}\end{bmatrix}, \tag{40}$$

where use has been made of (22), (27), (8) and (9). It is important to remark that the present displacement-based finite element description is prone to locking in the thin-shell limit. To remedy transverse shear locking of the 4-node element we apply the transverse shear modification proposed by Dvorkin and Bathe [18]. However, for simplicity of exposition, we keep the present displacement-based description. Substituting (39) into (36) yields

$$\sum_{A,B=1}^{n_{\text{node}}}\delta\boldsymbol{q}_A\cdot\boldsymbol{M}^{AB}\ddot{\boldsymbol{q}}_B+\sum_{A=1}^{n_{\text{node}}}\delta\boldsymbol{q}_A\cdot\left[\boldsymbol{F}^A_{\text{int}}-\boldsymbol{F}^A_{\text{ext}}\right]=0. \tag{41}$$

Note that the $\delta\boldsymbol{q}_A$'s in (41) are not independent but subject to the constraints in (34), i.e. $\delta\boldsymbol{q}\in T_q\mathrm{Q}_{\text{node}}$. Due to the unit-length condition on the nodal directors, there are at most five degrees of freedom per node. Let m be the total number of independent algebraic constraints so that the system under consideration has $\tilde{n}=6n_{\text{node}}-m$ degrees of freedom. Then $\delta\boldsymbol{q}\in T_q\mathrm{Q}_{\text{node}}$ can be written in the form

$$\delta\boldsymbol{q}=\boldsymbol{P}\delta\boldsymbol{v} \tag{42}$$

with independent variations $\delta\boldsymbol{v}\in\mathbb{R}^{\tilde{n}}$ and the $6n_{\text{node}}\times\tilde{n}$ matrix $\boldsymbol{P}$. Inserting (42) into (41) yields

$$\boldsymbol{P}^T[\boldsymbol{M}\ddot{\boldsymbol{q}}+\boldsymbol{F}_{\text{int}}-\boldsymbol{F}_{\text{ext}}]=0, \tag{43}$$

where the nodal vectors in (41) have been arranged in corresponding system vectors similar to (30). The semi-discrete equations of motion (43) can be regarded as ODEs on a manifold which determine $\boldsymbol{q}\in\mathrm{Q}_{\text{node}}$. This viewpoint is supported by the fact that the number of ODEs specified by (43) is equal to the dimension of the nodal configuration space (31), $\dim(\mathrm{Q}_{\text{node}})=\tilde{n}$.

Alternatively, the semi-discrete equations of motion can be written in the form of differential-algebraic equations (DAEs). To this end we introduce the $m\times6n_{\text{node}}$ constraint matrix

$$\boldsymbol{G}=\begin{bmatrix}\boldsymbol{G}_{\text{int}}\\ \boldsymbol{G}_{\text{ext}}\end{bmatrix}, \tag{44}$$

where $\boldsymbol{G}_{\text{ext}}$ is related to the external constraints and has already been introduced in (29). In addition to that, $\boldsymbol{G}_{\text{int}}=D\boldsymbol{\Phi}_{\text{int}}(\boldsymbol{q})$ corresponds to the internal constraints given by

$$\boldsymbol{\Phi}_{\text{int}}(\boldsymbol{q})=\boldsymbol{0}\quad\text{with}\ \Phi_{int_A}=\frac{1}{2}(\boldsymbol{d}_A\cdot\boldsymbol{d}_A-1) \tag{45}$$

for $A=1,2,\dots,n_{\text{node}}$. Note that the internal constraints are a consequence of the unit-length condition on the director field which is an intrinsic kinematic feature of the underlying shell theory. We further remark that, by design, the columns of matrix $\boldsymbol{P}$ span the null space of the constraint Jacobian $\boldsymbol{G}$, i.e. $\boldsymbol{GP}=\boldsymbol{0}$. Therefore, we shall refer to $\boldsymbol{P}$ occasionally as the null space matrix.

Now the semi-discrete shell problem can be cast in the following alternative DAE form: find $\boldsymbol{q}\in\mathbb{R}^{6n_{\text{node}}}$ such that

$$\begin{aligned}&\boldsymbol{M}\ddot{\boldsymbol{q}}+\boldsymbol{F}_{\text{int}}-\boldsymbol{F}_{\text{ext}}+\boldsymbol{G}^T\boldsymbol{\lambda}=\boldsymbol{0},\\ &\boldsymbol{G}_{\text{ext}}\boldsymbol{q}-\boldsymbol{b}=\boldsymbol{0},\\ &\boldsymbol{\Phi}_{\text{int}}=\boldsymbol{0}.\end{aligned} \tag{46}$$

The multipliers $\boldsymbol{\lambda}\in\mathbb{R}^m$ specify the forces of constraint necessary to enforce the m ideal holonomic constraints in $(46)_{2,3}$. A more compact form of the DAEs (46) can be obtained by introducing the vector of constraint functions

$$\boldsymbol{\Phi}(\boldsymbol{q}) = \begin{bmatrix} \boldsymbol{\Phi}_{\text{int}} \\ \boldsymbol{\Phi}_{\text{ext}} \end{bmatrix} \quad \text{with } \boldsymbol{\Phi}_{\text{ext}} = \boldsymbol{G}_{\text{ext}}\boldsymbol{q} - \boldsymbol{b} \tag{47}$$

along with the augmented potential function

$$\mathscr{V}_\lambda(\boldsymbol{q}) = V^h_{\text{int}}(\boldsymbol{q}) + V^h_{\text{ext}}(\boldsymbol{q}) + \sum_{l=1}^{m} \lambda^l \Phi_l(\boldsymbol{q}). \tag{48}$$

Now the DAEs (46) can be written in the alternative form

$$\boxed{\begin{aligned} &\dot{\boldsymbol{q}} - \boldsymbol{v} = \boldsymbol{0}, \\ &\boldsymbol{M}\dot{\boldsymbol{v}} + \nabla \mathscr{V}_\lambda(\boldsymbol{q}) = \boldsymbol{0}, \\ &\boldsymbol{\Phi}(\boldsymbol{q}) = \boldsymbol{0}. \end{aligned}} \tag{49}$$

Note that, with regard to (38), (44) and (47), the gradient of the augmented potential function may also be written in the form

$$\nabla \mathscr{V}_\lambda(\boldsymbol{q}) = \nabla V^h(\boldsymbol{q}) + \boldsymbol{G}^T\boldsymbol{\lambda}. \tag{50}$$

In the present work, the DAEs (49) provide the starting point for the time discretization dealt with in Section 4. We shall show subsequently that the present DAEs not only govern the motion of semi-discrete shells but also that of flexible multibody systems in general.

Remark 3.1. In the wake of recasting the present DAEs in the form (49), the vector of nodal velocities $\boldsymbol{v} \in T_q\mathsf{Q}_{\text{node}}$ has been introduced. The constraints on the velocities are often referred to as hidden constraints since they do not appear explicitly in the DAEs. Differentiating $(49)_3$ with respect to time yields the constraints on the velocity level given by $\boldsymbol{G}\boldsymbol{v} = \boldsymbol{0}$.

3.1. Conservation properties of the semi-discrete system

We next verify that the semi-discrete shell formulation inherits the conservation properties from the underlying continuous shell model (cf. Section 2.1).

3.1.1. Total linear momentum

If $\boldsymbol{F}_{\text{ext}} = \boldsymbol{0}$ and if no external constraints $\boldsymbol{\Phi}_{\text{ext}}$ act on the system then the total linear momentum is conserved. To verify this, one may insert $\delta\boldsymbol{q}_A = (\delta\boldsymbol{\varphi}_A, \delta\boldsymbol{d}_A) = (\boldsymbol{\xi}, \boldsymbol{0})$, with arbitrary and constant $\boldsymbol{\xi} \in \mathbb{R}^3$, into (41). Accordingly,

$$\boldsymbol{\xi} \cdot \left[\sum_{A,B=1}^{n_{\text{node}}} M^{AB}_{\varphi} \ddot{\boldsymbol{\varphi}}_B + \sum_{A=1}^{n_{\text{node}}} \boldsymbol{F}^A_{\text{int},\varphi} \right] = 0. \tag{51}$$

In this connection, $\boldsymbol{F}^A_{\text{int},\varphi}$ denotes the first three rows of the vector of nodal internal forces (40). Since $\sum N^A_{,\beta} = 0$, due to the completeness condition on the shape functions, i.e. $\sum N^A = 1$, $\sum \boldsymbol{F}^A_{\text{int},\varphi} = \boldsymbol{0}$. Thus (51) gives

$$\boldsymbol{\xi} \cdot \sum_{A,B=1}^{n_{\text{node}}} M^{AB}_{\varphi} \ddot{\boldsymbol{\varphi}}_B = \boldsymbol{\xi} \cdot \sum_{A=1}^{n_{\text{node}}} M^{A}_{\varphi} \ddot{\boldsymbol{\varphi}}_A = \boldsymbol{\xi} \cdot \frac{\mathrm{d}}{\mathrm{d}t}\boldsymbol{L}^h = 0, \tag{52}$$

where the discrete counterpart of the total linear momentum (14) is given by

$$\boldsymbol{L}^h = \sum_{A=1}^{n_{\text{node}}} M^A_{\varphi} \dot{\boldsymbol{\varphi}}_A \quad \text{with } M^A_{\varphi} = \sum_{B=1}^{n_{\text{node}}} M^{AB}_{\varphi} = \int_{\mathscr{S}^0} A_\varrho N^A \,\mathrm{d}\mathscr{S}. \tag{53}$$

In view of (52), $\boldsymbol{L}^h$ is conserved.

3.1.2. Total angular momentum

The discrete counterpart of the total angular momentum (16) can be written as

$$\boldsymbol{J}^h = \sum_{A=1}^{n_{\text{node}}} \left[\boldsymbol{\varphi}_A \times \boldsymbol{p}^A_{\varphi} + \boldsymbol{d}_A \times \boldsymbol{p}^A_d \right] \tag{54}$$

with

$$\boldsymbol{p}^A = \begin{bmatrix} \boldsymbol{p}^A_{\varphi} \\ \boldsymbol{p}^A_d \end{bmatrix} = \sum_{B=1}^{n_{\text{node}}} \boldsymbol{M}^{AB}\boldsymbol{v}_B. \tag{55}$$

Differentiating (54) with respect to time yields

$$\frac{\mathrm{d}}{\mathrm{d}t}\boldsymbol{J}^h = \sum_{A=1}^{n_{\text{node}}} \left[\boldsymbol{\varphi}_A \times \dot{\boldsymbol{p}}^A_{\varphi} + \boldsymbol{d}_A \times \dot{\boldsymbol{p}}^A_d \right]. \tag{56}$$

On the other hand, the semi-discrete equations of motion $(49)_2$ can also be written as

$$\begin{bmatrix} \dot{\boldsymbol{p}}^A_{\varphi} \\ \dot{\boldsymbol{p}}^A_d \end{bmatrix} = -\begin{bmatrix} \nabla_{\varphi_A} \mathscr{V}_\lambda \\ \nabla_{d_A} \mathscr{V}_\lambda \end{bmatrix} \tag{57}$$

for $A = 1, 2, \ldots, n_{\text{node}}$. Thus (56) can be recast in the form

$$\frac{\mathrm{d}}{\mathrm{d}t}\boldsymbol{J}^h = -\sum_{A=1}^{n_{\text{node}}} \left[\boldsymbol{\varphi}_A \times \nabla_{\varphi_A} \mathscr{V}_\lambda + \boldsymbol{d}_A \times \nabla_{d_A} \mathscr{V}_\lambda \right]. \tag{58}$$

Suppose that the underlying continuous system has a rotational symmetry. It can be easily verified that the corresponding semi-discrete system inherits the symmetry properties from the continuous one. In particular, the isoparametric interpolation (27) warrants that the discrete strains inherit the frame-indifference of the underlying continuous strains. To see this, consider rigid motions of the semi-discrete shell defined by

$$(\boldsymbol{\varphi}_A)^\sharp = \boldsymbol{c} + \boldsymbol{Q}\boldsymbol{\varphi}_A \quad \text{and} \quad (\boldsymbol{d}_A)^\sharp = \boldsymbol{Q}\boldsymbol{d}_A \tag{59}$$

for $\boldsymbol{c} \in \mathbb{R}^3$, $\boldsymbol{Q} \in \mathrm{SO}(3)$ and $A = 1, 2, \ldots, n_{\text{node}}$. Due to the isoparametric interpolation (27), the properties

$$\begin{aligned} &(\boldsymbol{\varphi}^h)^\sharp = \boldsymbol{c} + \boldsymbol{Q}\boldsymbol{\varphi}^h, \\ &(\boldsymbol{d}^h)^\sharp = \boldsymbol{Q}\boldsymbol{d}^h, \end{aligned} \tag{60}$$

hold in analogy to the continuous case, see Eq. (10). Accordingly, the invariance of the discrete strains can be shown along the lines of the continuous case treated above. Consequently, the potential function V^h_{int} inherits the rotational invariance from the stored energy function. That is, $V^h_{\text{int}}(\boldsymbol{Q} \circ \boldsymbol{q}) = V^h_{\text{int}}(\boldsymbol{q})$, where $\boldsymbol{Q} \circ \boldsymbol{q} = (\boldsymbol{Q}\boldsymbol{\varphi}_1, \boldsymbol{Q}\boldsymbol{d}_1, \ldots, \boldsymbol{Q}\boldsymbol{\varphi}_{n_{\text{node}}}, \boldsymbol{Q}\boldsymbol{d}_{n_{\text{node}}})$. Similarly, with regard to (45), the internal constraints on the nodal directors are rotationally invariant, i.e. $\Phi_{\text{int}_A}(\boldsymbol{Q}\boldsymbol{d}_A) = \Phi_{\text{int}_A}(\boldsymbol{d}_A)$.

Assume that the potential function V^h_{ext} accounting for the external loads is invariant under rotations about the axis $\boldsymbol{\xi} \in \mathbb{R}^3$, i.e. $V^h_{\text{ext}}(\boldsymbol{Q}_\varepsilon \circ \boldsymbol{q}) = V^h_{\text{ext}}(\boldsymbol{q})$, where $\boldsymbol{Q}_\varepsilon = \exp_{\mathrm{SO}(3)}(\varepsilon\widehat{\boldsymbol{\xi}}) \in \mathrm{SO}(3)$. For example, in the case of gravity loading, $\boldsymbol{\xi}$ is parallel to the vector of gravitational acceleration. Then the augmented potential function (48) shares the same property, i.e. $\mathscr{V}_\lambda(\boldsymbol{Q}_\varepsilon \circ \boldsymbol{q}) = \mathscr{V}_\lambda(\boldsymbol{q})$. Consequently,

$$\begin{aligned} 0 &= \frac{\mathrm{d}}{\mathrm{d}\varepsilon}\bigg|_{\varepsilon=0} \mathscr{V}_\lambda(\boldsymbol{Q}_\varepsilon \circ \boldsymbol{q}) \\ &= \sum_{A=1}^{n_{\text{node}}} \left[\nabla_{\varphi_A} \mathscr{V}_\lambda \cdot (\boldsymbol{\xi} \times \boldsymbol{\varphi}_A) + \nabla_{d_A} \mathscr{V}_\lambda \cdot (\boldsymbol{\xi} \times \boldsymbol{d}_A) \right] \\ &= \boldsymbol{\xi} \cdot \sum_{A=1}^{n_{\text{node}}} \left[\boldsymbol{\varphi}_A \times \nabla_{\varphi_A} \mathscr{V}_\lambda + \boldsymbol{d}_A \times \nabla_{d_A} \mathscr{V}_\lambda \right], \end{aligned} \tag{61}$$

and (58) yields

$$\boldsymbol{\xi} \cdot \frac{\mathrm{d}}{\mathrm{d}t}\boldsymbol{J}^h = 0. \tag{62}$$

Accordingly, the semi-discrete angular momentum map $J^h_{\boldsymbol{\xi}} = \boldsymbol{J}^h \cdot \boldsymbol{\xi}$ is a constant of the motion.

3.1.3. Total energy

With regard to (42), admissible nodal velocities $\boldsymbol{v} \in T_q \mathrm{Q}_{\mathrm{node}}$ can be written in the form

$$\boldsymbol{v} = \boldsymbol{P}\boldsymbol{\mu} \tag{63}$$

with independent velocities $\boldsymbol{\mu} \in \mathbb{R}^{\bar{n}}$. Pre-multiplying (43) by $\boldsymbol{\mu}$ yields

$$\begin{aligned} &\boldsymbol{v} \cdot [\boldsymbol{M}\dot{\boldsymbol{v}} + \boldsymbol{F}_{\mathrm{int}} - \boldsymbol{F}_{\mathrm{ext}}] = 0, \\ &\frac{\mathrm{d}}{\mathrm{d}t}\left[\frac{1}{2}\boldsymbol{v} \cdot \boldsymbol{M}\dot{\boldsymbol{v}}\right] + [\nabla V_{\mathrm{int}}(\boldsymbol{q}) + \nabla V_{\mathrm{ext}}(\boldsymbol{q})] \cdot \dot{\boldsymbol{q}} = 0, \\ &\frac{\mathrm{d}}{\mathrm{d}t} T^h(\boldsymbol{v}) + \frac{\mathrm{d}}{\mathrm{d}t} V^h(\boldsymbol{q}) = 0. \end{aligned} \tag{64}$$

In this connection, (38) and (39) have been taken into account. Moreover, the discrete counterpart of the kinetic energy (24) is given by

$$T^h(\boldsymbol{v}) = \frac{1}{2}\sum_{A,B=1}^{n_{\mathrm{node}}} \boldsymbol{v}_A \cdot \boldsymbol{M}^{AB}\boldsymbol{v}_B = \frac{1}{2}\boldsymbol{v} \cdot \boldsymbol{M}\boldsymbol{v}. \tag{65}$$

Accordingly, (64) corroborates that the total energy $T^h + V^h$ of the semi-discrete system is a conserved quantity.

4. Discretization in time

We next deal with the time discretization of the DAEs (49) governing the motion of the semi-discrete shell model. In particular, we aim at time-stepping schemes which inherit important conservation properties from the underlying finite-dimensional system.

4.1. Basic energy–momentum scheme

We make use of a direct discretization of the DAEs (49). In essence, we apply the conserving integration scheme proposed by Gonzalez [22], see also Betsch and Hesch [6, Section 3]. Consider a representative time interval $[t_n, t_{n+1}]$ with time step $\Delta t = t_{n+1} - t_n$, and given state-space coordinates $\boldsymbol{q}_n \in \mathrm{Q}_{\mathrm{node}}$ and $\boldsymbol{v}_n \in \mathbb{R}^{6n_{\mathrm{node}}}$ at t_n. The resulting algebraic problem to be solved is given as follows: find $(\boldsymbol{q}_{n+1}, \boldsymbol{v}_{n+1}) \in \mathbb{R}^{6n_{\mathrm{node}}} \times \mathbb{R}^{6n_{\mathrm{node}}}$ and $\boldsymbol{\lambda}_{n+1} \in \mathbb{R}^m$ as the solution of the algebraic system of equations

$$\begin{aligned} &\boldsymbol{q}_{n+1} - \boldsymbol{q}_n = \frac{\Delta t}{2}(\boldsymbol{v}_n + \boldsymbol{v}_{n+1}), \\ &\boldsymbol{M}(\boldsymbol{v}_{n+1} - \boldsymbol{v}_n) = -\Delta t \bar{\nabla}\mathscr{V}_{\lambda_{n+1}}(\boldsymbol{q}_n, \boldsymbol{q}_{n+1}), \\ &\boldsymbol{0} = \boldsymbol{\Phi}(\boldsymbol{q}_{n+1}). \end{aligned} \tag{66}$$

Note that, due to $(66)_3$, $\boldsymbol{q}_{n+1} \in \mathrm{Q}_{\mathrm{node}}$. In the sequel, the algorithm (66) will be called the basic energy–momentum (**BEM**) scheme. The advantageous algorithmic conservation properties of the BEM scheme are linked to the notion of a discrete gradient (or derivative) of a function $f : \mathbb{R}^k \mapsto \mathbb{R}$, introduced by Gonzalez [21]. In the present work $\bar{\nabla} f(\boldsymbol{q}_n, \boldsymbol{q}_{n+1})$ denotes the discrete gradient of f. The following properties of the discrete gradient play a fundamental role in the present work:

- If f is at most quadratic then the discrete gradient coincides with the standard gradient evaluated in the mid-point configuration specified by $\boldsymbol{q}_{n+\frac{1}{2}} = (\boldsymbol{q}_n + \boldsymbol{q}_{n+1})/2$. That is, in this case $\bar{\nabla} f(\boldsymbol{q}_n, \boldsymbol{q}_{n+1}) = \nabla f\left(\boldsymbol{q}_{n+\frac{1}{2}}\right)$.
- Satisfaction of the directionality property:

$$\bar{\nabla} f(\boldsymbol{q}_n, \boldsymbol{q}_{n+1}) \cdot [\boldsymbol{q}_{n+1} - \boldsymbol{q}_n] = f(\boldsymbol{q}_{n+1}) - f(\boldsymbol{q}_n). \tag{67}$$

- Major symmetry properties are inherited from the underlying time continuous system. In particular, it will be shown in Section 4.3.2 that a time discrete version of (61) is satisfied.

With regard to the augmented potential function (48), application of the discrete gradient in $(66)_2$ yields

$$\begin{aligned} \bar{\nabla}\mathscr{V}_{\lambda_{n+1}}(\boldsymbol{q}_n, \boldsymbol{q}_{n+1}) &= \bar{\nabla} V^h_{\mathrm{int}}(\boldsymbol{q}_n, \boldsymbol{q}_{n+1}) + \nabla V^h_{\mathrm{ext}}\left(\boldsymbol{q}_{n+\frac{1}{2}}\right) \\ &\quad + \sum_{l=1}^{m} (\lambda_l)_{n+1} \nabla \Phi_l\left(\boldsymbol{q}_{n+\frac{1}{2}}\right) \\ &= \mathbf{F}_{\mathrm{int}}(\boldsymbol{q}_n, \boldsymbol{q}_{n+1}) - \boldsymbol{F}_{\mathrm{ext}}\left(t_{n+\frac{1}{2}}\right) + \boldsymbol{G}\left(\boldsymbol{q}_{n+\frac{1}{2}}\right)^T \boldsymbol{\lambda}_{n+1}. \end{aligned} \tag{68}$$

The nodal contributions to the discrete version of the internal force vector $\mathbf{F}_{\mathrm{int}}(\boldsymbol{q}_n, \boldsymbol{q}_{n+1})$ follow from the following definition of the discrete counterpart of the internal nodal forces (40):

$$\mathbf{F}^A_{\mathrm{int}}(\boldsymbol{q}_n, \boldsymbol{q}_{n+1}) = \begin{bmatrix} \int_{\mathscr{S}^0} \left[\left(\boldsymbol{\varphi}^h_{,\alpha}\right)_{n+\frac{1}{2}} n^{\alpha\beta} + \left(\boldsymbol{d}^h_{,\alpha}\right)_{n+\frac{1}{2}} m^{\alpha\beta} + \left(\boldsymbol{d}^h\right)_{n+\frac{1}{2}} q^{\beta}\right] N_{A,\beta}\, \mathrm{d}\mathscr{S} \\ \int_{\mathscr{S}^0} \left[m^{\alpha\beta} N_{A,\beta} + q^{\alpha} N_A\right] \left(\boldsymbol{\varphi}^h_{,\alpha}\right)_{n+\frac{1}{2}} \mathrm{d}\mathscr{S} \end{bmatrix}. \tag{69}$$

In this connection, $n^{\alpha\beta}$, $m^{\alpha\beta}$, and q^{β} are algorithmic stress resultants. For general stored energy functions, the algorithmic stress resultants can be calculated as described in Appendix A. For the customary St. Venant–Kirchhoff-type constitutive model, the algorithmic stress resultants assume a particularly simple form as will be outlined next.

Remark 4.1. Although the BEM scheme ensures that $\boldsymbol{q}_{n+1} \in \mathrm{Q}_{\mathrm{node}}$, in general $\boldsymbol{v}_{n+1} \notin T_{q_{n+1}}\mathrm{Q}_{\mathrm{node}}$. The nodal constraints on the velocity level can be enforced at the end of the time step by adjusting the GGL-type [19] technique to the present conserving framework, see [8] for further details. However, numerical tests revealed no significant improvement of the numerical performance which would justify the additional computational effort.

4.1.1. Isotropic constitutive equations

A common constitutive model for isotropic hyperelastic material response is governed by the decoupled stored energy function

$$\begin{aligned} W &= \overline{W}\left(\varepsilon_{\alpha\beta}, \rho_{\alpha\beta}, \delta_\alpha\right) \\ &= \frac{1}{2} H_m^{\alpha\beta\gamma\delta} \varepsilon_{\alpha\beta}\varepsilon_{\gamma\delta} + \frac{1}{2} H_b^{\alpha\beta\gamma\delta} \rho_{\alpha\beta}\rho_{\gamma\delta} + \frac{1}{2} Q^{\alpha\beta}\delta_\alpha\delta_\beta, \end{aligned} \tag{70}$$

where $\varepsilon_{\alpha\beta} = \frac{1}{2}\left[a_{\alpha\beta} - a^0_{\alpha\beta}\right]$ are the membrane strains, $\rho_{\alpha\beta} = \frac{1}{2}\left[\kappa_{\alpha\beta} - \kappa^0_{\alpha\beta}\right]$ are the bending strains, and $\delta_\alpha = \gamma_\alpha - \gamma^0_\alpha$ are the transverse shear strains. Here and in the sequel, index 0 refers to quantities in the stress-free initial configuration at time t_0. In (70),

$$\begin{aligned} H_m^{\alpha\beta\gamma\delta} &= \frac{Eh}{1-\nu^2} H^{\alpha\beta\gamma\delta}, \\ H_b^{\alpha\beta\gamma\delta} &= \frac{Eh^3}{12(1-\nu^2)} H^{\alpha\beta\gamma\delta} \end{aligned} \tag{71}$$

and $Q^{\alpha\beta} = \frac{5Eh}{6(2+2\nu)} a_0^{\alpha\beta}$. In this connection, $[a_0^{\alpha\beta}] = [a^0_{\alpha\beta}]^{-1}$, with metric coefficients $a^0_{\alpha\beta} = \boldsymbol{\varphi}^h_{0,\alpha} \cdot \boldsymbol{\varphi}^h_{0,\beta}$, associated with the reference surface of the shell at time t_0. Moreover, E is Young's modulus, ν is Poisson's ratio, and h denotes the thickness of the shell. Inserting expression (70) into the formulas for the calculation of the algorithmic stress resultants (see Eq. (A.1) in Appendix A) yields

$$\begin{aligned} n^{\alpha\beta} &= H_n^{\alpha\beta\gamma\delta} \frac{1}{2}\left[(\varepsilon_{\gamma\delta})_n + (\varepsilon_{\gamma\delta})_{n+1}\right], \\ m^{\alpha\beta} &= H_b^{\alpha\beta\gamma\delta} \frac{1}{2}\left[(\rho_{\gamma\delta})_n + (\rho_{\gamma\delta})_{n+1}\right], \\ q^{\beta} &= Q^{\beta\alpha} \frac{1}{2}\left[(\delta_\alpha)_n + (\delta_\alpha)_{n+1}\right]. \end{aligned} \tag{72}$$

4.2. Reduced energy–momentum scheme

To reduce the computational costs and improve the conditioning of the algebraic system to be solved we perform a size-reduction of the BEM scheme. The size-reduction procedure rest on (i) the introduction of a matrix $\mathbf{P}(\boldsymbol{q}_n, \boldsymbol{q}_{n+1})$, the columns of which span the null space of the discrete constraint Jacobian in (68), so that the relationship

$$\boldsymbol{G}\left(\boldsymbol{q}_{n+\frac{1}{2}}\right)\mathbf{P}(\boldsymbol{q}_n, \boldsymbol{q}_{n+1}) = \boldsymbol{0} \tag{73}$$

is satisfied, and (ii) a parametrization of the nodal configuration space $\mathrm{Q}_{\mathrm{node}}$ in the neighborhood of $\boldsymbol{q}_n \in \mathrm{Q}_{\mathrm{node}}$. Let the corresponding map $\boldsymbol{F}_{q_n} : \mathrm{U} \mapsto \mathrm{Q}_{\mathrm{node}}$ be given in terms of local coordinates $\boldsymbol{u} \in \mathrm{U} \subset \mathbb{R}^{\bar{n}}$. Then the redundant coordinates $\boldsymbol{q}_{n+1} \in \mathbb{R}^{6n_{\mathrm{node}}}$ can be expressed in terms of new incremental unknowns $\boldsymbol{u} \in \mathrm{U}$ through

$$\boldsymbol{q}_{n+1} = \boldsymbol{F}_{q_n}(\boldsymbol{u}). \tag{74}$$

Now the reduced energy–momentum (**REM**) scheme can be directly deduced from the BEM scheme leading to the following algebraic problem: Given $\boldsymbol{q}_n \in \mathrm{Q}_{\mathrm{node}}$ and $\boldsymbol{v}_n \in \mathbb{R}^{6n_{\mathrm{node}}}$, find $\boldsymbol{u} \in \mathrm{U}$ and $\boldsymbol{v}_{n+1} \in \mathbb{R}^{6n_{\mathrm{node}}}$ as the solution of

$$\begin{aligned} &\boldsymbol{q}_{n+1} - \boldsymbol{q}_n = \frac{\Delta t}{2}(\boldsymbol{v}_n + \boldsymbol{v}_{n+1}), \\ &\mathbf{P}(\boldsymbol{q}_n, \boldsymbol{q}_{n+1})^T \boldsymbol{M}(\boldsymbol{v}_{n+1} - \boldsymbol{v}_n) = \Delta t\left[\boldsymbol{F}_{\mathrm{ext}}\left(t_{n+\frac{1}{2}}\right) - \mathbf{F}_{\mathrm{int}}(\boldsymbol{q}_n, \boldsymbol{q}_{n+1})\right], \end{aligned} \tag{75}$$

where $\boldsymbol{q}_{n+1} \in \mathrm{Q}_{\mathrm{node}}$ is represented by (74). It can be easily verified that the REM scheme is equivalent to the BEM scheme, see [5, Section 3.4] for details.

4.3. Algorithmic conservation properties

This section contains a verification of the algorithmic conservation properties of the advocated energy–momentum scheme.

4.3.1. Total linear momentum

Algorithmic conservation of linear momentum can be verified along the lines of the semi-discrete case dealt with in Section 3.1.1. In view of (53),

$$\begin{aligned} \xi \cdot \left[\boldsymbol{L}^h_{n+1} - \boldsymbol{L}^h_n\right] &= \xi \cdot \sum_{A=1}^{n_{\mathrm{node}}} M^A_\varphi \left[\boldsymbol{v}^\varphi_{An+1} - \boldsymbol{v}^\varphi_{An}\right] \\ &= \xi \cdot \sum_{A,B=1}^{n_{\mathrm{node}}} M^{AB}_\varphi \left[\boldsymbol{v}^\varphi_{An+1} - \boldsymbol{v}^\varphi_{An}\right] \\ &= \xi \cdot \sum_{A=1}^{n_{\mathrm{node}}} \left[\boldsymbol{p}^A_{\varphi n+1} - \boldsymbol{p}^A_{\varphi n}\right] = -\Delta t \xi \cdot \sum_{A=1}^{n_{\mathrm{node}}} \bar{\nabla}_{\varphi_A} \mathscr{V}_{\lambda_{n+1}}. \end{aligned} \tag{76}$$

Provided that $\xi \cdot \sum \bar{\nabla}_{\varphi_A} V^h_{\mathrm{ext}} = 0$ together with $\xi \cdot \bar{\nabla}_{\varphi_A} \boldsymbol{\Phi}_{\mathrm{ext}} = 0$, and since, as in the semi-discrete case, $\sum \bar{\nabla}_{\varphi_A} V^h_{\mathrm{int}} = \boldsymbol{0}$, the right-hand side of (76) vanishes, which confirms algorithmic conservation of linear momentum.

4.3.2. Total angular momentum

Starting with expression (54) for the total angular momentum pertaining to the semi-discrete shell, a straightforward calculation yields

$$\begin{aligned} \boldsymbol{J}^h_{n+1} - \boldsymbol{J}^h_n &= \sum_{A=1}^{n_{\mathrm{node}}} \left[\boldsymbol{\varphi}_{An+1} \times \boldsymbol{p}^A_{\varphi n+1} - \boldsymbol{\varphi}_{An} \times \boldsymbol{p}^A_{\varphi n} + \boldsymbol{d}_{An+1} \times \boldsymbol{p}^A_{dn+1} - \boldsymbol{d}_{An} \times \boldsymbol{p}^A_{dn}\right] \\ &= \sum_{A=1}^{n_{\mathrm{node}}} \left\{\boldsymbol{\varphi}_{An+\frac{1}{2}} \times \left[\boldsymbol{p}^A_{\varphi n+1} - \boldsymbol{p}^A_{\varphi n}\right] + \left[\boldsymbol{\varphi}_{An+1} - \boldsymbol{\varphi}_{An}\right] \times \boldsymbol{p}^A_{\varphi n+\frac{1}{2}} + \boldsymbol{d}_{An+\frac{1}{2}} \right. \\ &\quad \left. \times \left[\boldsymbol{p}^A_{dn+1} - \boldsymbol{p}^A_{dn}\right] + \left[\boldsymbol{d}_{An+1} - \boldsymbol{d}_{An}\right] \times \boldsymbol{p}^A_{dn+\frac{1}{2}}\right\}. \end{aligned} \tag{77}$$

Similar to (57), the discrete equations of motion $(66)_2$ can be written in the alternative form

$$\begin{bmatrix} \boldsymbol{p}^A_{\varphi n+1} - \boldsymbol{p}^A_{\varphi n} \\ \boldsymbol{p}^A_{dn+1} - \boldsymbol{p}^A_{dn} \end{bmatrix} = -\Delta t \begin{bmatrix} \bar{\nabla}_{\varphi_A} \mathscr{V}_{\lambda_{n+1}} \\ \bar{\nabla}_{d_A} \mathscr{V}_{\lambda_{n+1}} \end{bmatrix} \tag{78}$$

for $A = 1, 2, \ldots, n_{\mathrm{node}}$. In addition to that, $(66)_1$ can also be written as

$$\begin{bmatrix} \boldsymbol{\varphi}_{An+1} - \boldsymbol{\varphi}_{An} \\ \boldsymbol{d}_{An+1} - \boldsymbol{d}_{An} \end{bmatrix} = \Delta t \begin{bmatrix} \boldsymbol{v}^\varphi_{An+\frac{1}{2}} \\ \boldsymbol{v}^d_{An+\frac{1}{2}} \end{bmatrix} \tag{79}$$

for $A = 1, 2, \ldots, n_{\mathrm{node}}$. Inserting from (78) and (79) into (77) yields

$$\begin{aligned} \boldsymbol{J}^h_{n+1} - \boldsymbol{J}^h_n = &-\Delta t \sum_{A=1}^{n_{\mathrm{node}}} \left\{\boldsymbol{\varphi}_{An+\frac{1}{2}} \times \bar{\nabla}_{\varphi_A} \mathscr{V}_{\lambda_{n+1}} + \boldsymbol{d}_{An+\frac{1}{2}} \times \bar{\nabla}_{d_A} \mathscr{V}_{\lambda_{n+1}}\right\} \\ &+ \Delta t \sum_{A,B=1}^{n_{\mathrm{node}}} \left\{M^{AB}_\varphi \boldsymbol{v}^\varphi_{An+\frac{1}{2}} \times \boldsymbol{v}^\varphi_{Bn+\frac{1}{2}} + M^{AB}_d \boldsymbol{v}^d_{An+\frac{1}{2}} \times \boldsymbol{v}^d_{An+\frac{1}{2}}\right\}, \end{aligned} \tag{80}$$

where use has been made of (55) and (37). In the above equation the second sum vanishes due to the symmetry of the inertial quantities M^{AB}_φ, M^{AB}_d and the skew-symmetry of the cross product. Accordingly, the discrete counterpart of (58) can be written as

$$\boldsymbol{J}^h_{n+1} - \boldsymbol{J}^h_n = -\Delta t \sum_{A=1}^{n_{\mathrm{node}}} \left\{\boldsymbol{\varphi}_{An+\frac{1}{2}} \times \bar{\nabla}_{\varphi_A} \mathscr{V}_{\lambda_{n+1}} + \boldsymbol{d}_{An+\frac{1}{2}} \times \bar{\nabla}_{d_A} \mathscr{V}_{\lambda_{n+1}}\right\}. \tag{81}$$

On the other hand, it can be easily verified by a straightforward calculation starting with (68) that, under the same symmetry assumptions which led to the result (61), the following equation holds in the fully discrete case:

$$\xi \cdot \sum_{A=1}^{n_{\mathrm{node}}} \left\{\boldsymbol{\varphi}_{An+\frac{1}{2}} \times \bar{\nabla}_{\varphi_A} \mathscr{V}_{\lambda_{n+1}} + \boldsymbol{d}_{An+\frac{1}{2}} \times \bar{\nabla}_{d_A} \mathscr{V}_{\lambda_{n+1}}\right\} = 0. \tag{82}$$

Accordingly,

$$\xi \cdot \left[\boldsymbol{J}^h_{n+1} - \boldsymbol{J}^h_n\right] = 0, \tag{83}$$

which confirms algorithm conservation of angular momentum.

4.3.3. Total energy

For autonomous systems, algorithmic conservation of energy can be easily verified by scalar multiplying $(66)_2$ by $\boldsymbol{v}_{n+\frac{1}{2}}$ and taking into account $(66)_1$:

$$\begin{aligned} &\boldsymbol{v}_{n+\frac{1}{2}} \cdot \boldsymbol{M}(\boldsymbol{v}_{n+1} - \boldsymbol{v}_n) = -\bar{\nabla} \mathscr{V}_{\lambda_{n+1}}(\boldsymbol{q}_n, \boldsymbol{q}_{n+1}) \cdot \left[\boldsymbol{q}_{n+1} - \boldsymbol{q}_n\right], \\ &T^h(\boldsymbol{v}_{n+1}) - T^h(\boldsymbol{v}_n) = -\left[\mathscr{V}_{\lambda_{n+1}}(\boldsymbol{q}_{n+1}) - \mathscr{V}_{\lambda_{n+1}}(\boldsymbol{q}_n)\right], \\ &T^h(\boldsymbol{v}_{n+1}) + V^h(\boldsymbol{q}_{n+1}) - \left[T^h(\boldsymbol{v}_n) + V^h(\boldsymbol{q}_n)\right] \\ &\quad = -\sum_{l=1}^{m} \lambda^l_{n+1}\left[\Phi_l(\boldsymbol{q}_{n+1}) - \Phi_l(\boldsymbol{q}_n)\right], \end{aligned} \tag{84}$$

where use has been made of (65), (48), and (38) and the directionality property (67) of the discrete gradient. Since the algebraic constraints are satisfied at t_n and t_{n+1}, the right-hand side of the above equation vanishes. Accordingly, the scheme conserves total energy.

5. Model problem

In the DAEs (49) governing the motion of the semi-discrete shell the unit-length constraint on the nodal directors is enforced by means of nodal constraint forces. As has been outlined in Section 4.2, the algorithmic forces of constraint can be eliminated from the BEM scheme leading to the REM scheme. This section contains a detailed treatment of this approach.

Since the constraints are confined to the nodes we introduce a simple model problem which captures the essential features and facilitates a concise exposition. In addition to that, the model

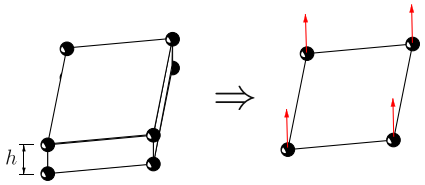

Fig. 3. Illustration of the degeneration process: 4-node shell element based on a 8-node continuum element.

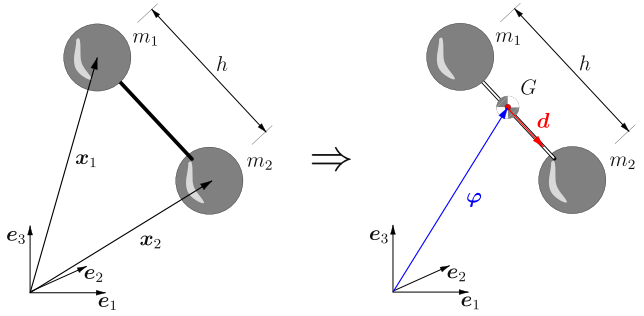

Fig. 4. The dumbbell in terms of Cartesian coordinates (left) and shell-type coordinates (right).

problem serves the purpose of comparing our approach to the more common method of introducing rotational parameters *prior* to the time discretization. In the context of the model problem we further provide a detailed description of the implementation of the resulting algorithms which can be easily generalized to the shell problem.

The model problem is motivated by the degenerated continuum approach which relies on imposing the constraints of the shell theory on a continuum element. In the wake of this process the two nodes along a fiber of a continuum element are replaced by one node with associated director, see Fig. 3. Correspondingly, the model problem consists of a dumbbell whose configuration is originally described in terms of Cartesian coordinates which specify the position vectors $\boldsymbol{x}_1, \boldsymbol{x}_2 \in \mathbb{R}^3$ of the two mass points m_1 and m_2 (Fig. 4).

The distance h between the two masses is assumed to be constant which corresponds to the inextensibility condition in the shell theory. The kinetic energy $\overline{T}$, potential $\overline{V}$ and internal constraint function $\overline{\Phi}_{\text{int}}$ are given by

$$\begin{aligned} \overline{T} &= \frac{1}{2} m_1 \|\dot{\boldsymbol{x}}_1\|^2 + m_2 \|\dot{\boldsymbol{x}}_2\|^2, \\ \overline{V} &= \overline{\mathscr{V}}(\boldsymbol{x}_1, \boldsymbol{x}_2), \\ \overline{\Phi}_{\text{int}} &= \frac{1}{2} \left(\|\boldsymbol{x}_2 - \boldsymbol{x}_1\|^2 / h^2 - 1 \right). \end{aligned} \tag{85}$$

The total linear momentum $\overline{\boldsymbol{L}}$ and angular momentum $\overline{\boldsymbol{J}}$ with respect to the origin assume the form

$$\begin{aligned} \overline{\boldsymbol{L}} &= m_1 \dot{\boldsymbol{x}}_1 + m_2 \dot{\boldsymbol{x}}_2, \\ \overline{\boldsymbol{J}} &= m_1 \boldsymbol{x}_1 \times \dot{\boldsymbol{x}}_1 + m_2 \boldsymbol{x}_2 \times \dot{\boldsymbol{x}}_2. \end{aligned} \tag{86}$$

The introduction of shell-type coordinates rests on the center of mass $\boldsymbol{\varphi} \in \mathbb{R}^3$ and director $\boldsymbol{d} \in \mathbb{R}^3$, defined by the relationships

$$\boldsymbol{\varphi} = \frac{m_1 \boldsymbol{x}_1 + m_2 \boldsymbol{x}_2}{m_1 + m_2} \quad \text{and} \quad \boldsymbol{d} = \frac{\boldsymbol{x}_2 - \boldsymbol{x}_1}{h}. \tag{87}$$

The quantities in (85) now assume the modified form

$$\begin{aligned} \overline{T} &= \frac{1}{2} \overline{A}_\varrho \|\dot{\boldsymbol{\varphi}}\|^2 + \frac{1}{2} \overline{I}_\varrho \|\dot{\boldsymbol{d}}\|^2, \\ \overline{V} &= \overline{V}(\boldsymbol{\varphi}, \boldsymbol{d}), \\ \overline{\Phi}_{\text{int}} &= \frac{1}{2} \left(\|\boldsymbol{d}\|^2 - 1 \right) \end{aligned} \tag{88}$$

with inertial quantities

$$\overline{A}_\varrho = m_1 + m_2 \quad \text{and} \quad \overline{I}_\varrho = \frac{m_1 m_2}{m_1 + m_2} h^2. \tag{89}$$

The linear and angular momenta are now given by

$$\begin{aligned} \overline{\boldsymbol{L}} &= \overline{A}_\varrho \dot{\boldsymbol{\varphi}}, \\ \overline{\boldsymbol{J}} &= \overline{A}_\varrho \boldsymbol{\varphi} \times \dot{\boldsymbol{\varphi}} + \overline{\boldsymbol{J}}_\varphi, \end{aligned} \tag{90}$$

where $\overline{\boldsymbol{J}}_\varphi$ is the spin angular momentum

$$\overline{\boldsymbol{J}}_\varphi = \overline{I}_\varrho \boldsymbol{d} \times \dot{\boldsymbol{d}}. \tag{91}$$

The equations of motion pertaining to the dumbbell can now be easily derived from Lagrange's equations leading to

$$\begin{aligned} &\overline{A}_\varrho \ddot{\boldsymbol{\varphi}} + \nabla_\varphi \overline{V} = \boldsymbol{0}, \\ &\overline{I}_\varrho \ddot{\boldsymbol{d}} + \lambda_1 \boldsymbol{d} + \nabla_d \overline{V} = \boldsymbol{0}, \\ &\frac{1}{2} \left(\|\boldsymbol{d}\|^2 - 1 \right) = 0. \end{aligned} \tag{92}$$

Note that the above system of equations fits perfectly into the framework for DAEs specified by (49). In what follows we shall focus on the rotational motion of the dumbbell which is governed by $(92)_{2,3}$. The algebraic constraint $(92)_3$ confines possible director configurations to the nonlinear manifold $\mathrm{S}^2 \subset \mathbb{R}^3$. The DAEs $(92)_{2,3}$ can thus be viewed as ODEs on the manifold S^2.

5.1. Connection between S^2 and $SO(3)$

As outlined above, the unit-length constraint $(92)_3$ restricts the rotational motion of the dumbbell to a two-dimensional configuration space, i.e. $\boldsymbol{d}(t) \in \mathrm{S}^2$. The consistency condition $d\overline{\Phi}_{\text{int}}/dt = 0$ yields an additional constraint on the velocity level. That is, possible director velocities have to lie in the tangent space $T_d\mathrm{S}^2$. Consequently, admissible director velocities $\boldsymbol{v} \in T_d\mathrm{S}^2$ can be written in the form

$$\boldsymbol{v} = V_1 \boldsymbol{d}_1 + V_2 \boldsymbol{d}_2, \tag{93}$$

where $\boldsymbol{d}_1, \boldsymbol{d}_2 \in \mathbb{R}^3$ span the orthogonal complement of the line along $\boldsymbol{d}$. We choose $\boldsymbol{d}_1$ and $\boldsymbol{d}_2$ such that $\{\boldsymbol{d}_1, \boldsymbol{d}_2, \boldsymbol{d}\}$ form a right-handed orthonormal frame. Note that the representation (93) contains two independent 'generalized speeds' $V_1, V_2 \in \mathbb{R}$, which conforms with the fact that $\dim(T_d\mathrm{S}^2)$=2. Possible configurations of the rotated director may be characterized by parameter curves of the form

$$\boldsymbol{d}_\epsilon = \exp_d(\varepsilon \boldsymbol{v}) = \exp_{\mathrm{SO}(3)}(\varepsilon \widehat{\omega}) \boldsymbol{d} \tag{94}$$

for $\boldsymbol{v} \in T_d\mathrm{S}^2$. Here, $\exp_d : T_d\mathrm{S}^2 \mapsto \mathrm{S}^2$ denotes the exponential map on the unit sphere given by

$$\exp_d(\varepsilon \boldsymbol{v}) = \cos(\varepsilon \|\boldsymbol{v}\|) \boldsymbol{d} + \frac{\sin(\varepsilon \|\boldsymbol{v}\|)}{\|\boldsymbol{v}\|} \boldsymbol{v}. \tag{95}$$

Furthermore, in (94), $\exp_{\mathrm{SO}(3)} : \mathrm{so}(3) \mapsto \mathrm{SO}(3)$ is the exponential map on the rotation group $\mathrm{SO}(3)$, given by the Rodrigues formula (see, e.g., Marsden and Ratiu [32])

$$\exp_{\mathrm{SO}(3)}(\varepsilon \widehat{\omega}) = \boldsymbol{I} + \frac{\sin(\varepsilon \|\boldsymbol{\omega}\|)}{\|\boldsymbol{\omega}\|} \widehat{\omega} + \frac{1}{2} \left[\frac{\sin(\varepsilon \|\boldsymbol{\omega}\|/2)}{\|\boldsymbol{\omega}/2\|} \right]^2 \widehat{\theta}^2. \tag{96}$$

In this connection $\widehat{\omega} \in \mathrm{so}(3)$ is a skew-symmetric matrix with associated axial vector $\boldsymbol{\omega} \in \mathbb{R}^3$. That is, $\widehat{\omega}\boldsymbol{a} = \boldsymbol{\omega} \times \boldsymbol{a}$ for any $\boldsymbol{a} \in \mathbb{R}^3$. Due to the properties of the exponential map, (94) implies

$$\boldsymbol{d}_\epsilon|_{\varepsilon=0} = \boldsymbol{d} \tag{97}$$

and

$$\frac{\mathrm{d}}{\mathrm{d}\varepsilon}\bigg|_{\varepsilon=0} \boldsymbol{d}_\epsilon = \boldsymbol{v} = \widehat{\omega} \boldsymbol{d}. \tag{98}$$

Accordingly,

$$\boldsymbol{v} = \boldsymbol{\omega} \times \boldsymbol{d}. \tag{99}$$

Taking the cross product with $\boldsymbol{d}$ from the left yields

$$\boldsymbol{d} \times \boldsymbol{v} = \boldsymbol{d} \times (\boldsymbol{\omega} \times \boldsymbol{d}) = \|\boldsymbol{d}\|^2 \boldsymbol{\omega} - (\boldsymbol{d} \cdot \boldsymbol{\omega})\boldsymbol{d}. \tag{100}$$

Under the assumption of vanishing drill rotations, i.e.

$$\boldsymbol{d} \cdot \boldsymbol{\omega} = 0. \tag{101}$$

Eq. (100) determines the angular velocity vector $\boldsymbol{\omega}$ associated with $\boldsymbol{v} \in T_d\mathrm{S}^2$:

$$\boldsymbol{\omega} = \boldsymbol{d} \times \boldsymbol{v}. \tag{102}$$

Inserting from (93) into the last equation yields

$$\boldsymbol{\omega} = \Omega_1 \boldsymbol{d}_1 + \Omega_2 \boldsymbol{d}_2 \tag{103}$$

with

$$\begin{aligned} \Omega_1 &= -V_2, \\ \Omega_2 &= V_1. \end{aligned} \tag{104}$$

To summarize, the rotational motion on S^2 can be described as drill-free rotation on SO(3) in terms of two independent rotational degrees of freedom. In particular, the director motion is accompanied by the rotation of the triad $\{\boldsymbol{d}_1, \boldsymbol{d}_2, \boldsymbol{d}_3 \equiv \boldsymbol{d}\}$, with corresponding parameter curves

$$\boldsymbol{d}_{i\epsilon} = \exp_{\mathrm{SO(3)}}(\varepsilon \widehat{\boldsymbol{\omega}}) \boldsymbol{d}_i \tag{105}$$

for $i = 1, 2, 3$.

5.2. Size-reduction of the rotational equations of motion

We next perform a size-reduction of the original DAEs $(92)_{2,3}$ governing the rotational motion of the dumbbell. In particular, the size-reduction rests on the introduction of a matrix $\overline{\boldsymbol{\Lambda}}$, whose columns span the null space of the constraint Jacobian $D\overline{\Phi}_{\mathrm{int}}(\boldsymbol{d}) = \boldsymbol{d}^T$. According to (99) and (93), admissible director velocities $\dot{\boldsymbol{d}} \in T_d\mathrm{S}^2$ may be written in the form

$$\dot{\boldsymbol{d}} = \boldsymbol{\omega} \times \boldsymbol{d} = \overline{\boldsymbol{\Lambda}} \boldsymbol{V}, \tag{106}$$

where

$$\overline{\boldsymbol{\Lambda}} = [\, \boldsymbol{d}_1 \quad \boldsymbol{d}_2 \,] \quad \text{and} \quad \boldsymbol{V} = \begin{bmatrix} V_1 \\ V_2 \end{bmatrix}. \tag{107}$$

Accordingly, the 3×2 matrix $\overline{\boldsymbol{\Lambda}}$ plays the role of a null space matrix introduced in (42). Differentiating (106) with respect to time yields

$$\ddot{\boldsymbol{d}} = \dot{\boldsymbol{\omega}} \times \boldsymbol{d} - \|\boldsymbol{\omega}\|^2 \boldsymbol{d}, \tag{108}$$

where use has been made of condition (101). To perform the size-reduction we insert (108) into $(92)_2$ and premultiply the resulting equation by $\overline{\boldsymbol{\Lambda}}^T$. Accordingly, we get

$$\boxed{[\, \boldsymbol{d}_1 \quad \boldsymbol{d}_2 \,]^T (\bar{I}_\varrho \dot{\boldsymbol{\omega}} \times \boldsymbol{d} + \nabla_d \overline{V}) = \boldsymbol{0}} \tag{109}$$

with $[\boldsymbol{d}_1, \boldsymbol{d}_2, \boldsymbol{d}] \in SO(3)$. The two equations in (109) constitute nonlinear ODEs on S^2. These ODEs determine the (drill-free about $\boldsymbol{d}$) motion of the triad $\{\boldsymbol{d}_1, \boldsymbol{d}_2, \boldsymbol{d}\}$. Note that expression (91) for the spin angular momentum can be rewritten as

$$\bar{\boldsymbol{J}}_\varphi = \bar{I}_\varrho \boldsymbol{\omega}, \tag{110}$$

where (102) has been taken into account. Furthermore, since $\|\dot{\boldsymbol{d}}\|^2 = \|\boldsymbol{\omega} \times \boldsymbol{d}\|^2 = \boldsymbol{\omega} \cdot [\boldsymbol{d} \times (\boldsymbol{\omega} \times \boldsymbol{d})] = \|\boldsymbol{\omega}\|^2$, the kinetic energy $(88)_1$ can be recast in the form

$$\overline{T} = \frac{1}{2} \overline{A}_\varrho \|\dot{\boldsymbol{\varphi}}\|^2 + \frac{1}{2} \bar{I}_\varrho \|\boldsymbol{\omega}\|^2. \tag{111}$$

Remark 5.1. An alternative form of (109) can be obtained by cross-multiplying $(92)_2$ by $\boldsymbol{d}$ and taking into account expression (102), which implies that $\boldsymbol{d} \times \ddot{\boldsymbol{d}} = \dot{\boldsymbol{\omega}}$. Accordingly, $(92)_2$ yields

$$\bar{I}_\varrho \dot{\boldsymbol{\omega}} + \boldsymbol{d} \times \nabla_d \overline{V} = \boldsymbol{0}. \tag{112}$$

This relationship yields two independent equations which are equivalent to (109).

5.3. Discretization of the ODEs on S^2

We next apply the angular momentum conserving time-stepping scheme developed by Simo et al. [38] to the ODEs (109) on S^2. The scheme can be viewed as midpoint rule on S^2. The time discrete version of (109) reads

$$\left[(\boldsymbol{d}_1)_{n+\frac{1}{2}} \quad (\boldsymbol{d}_2)_{n+\frac{1}{2}} \right]^T \left(\bar{I}_\varrho (\boldsymbol{\omega}_{n+1} - \boldsymbol{\omega}_n) \times \boldsymbol{d}_{n+\frac{1}{2}} + \Delta t \nabla_d V|_{n+\frac{1}{2}} \right) = \boldsymbol{0} \tag{113}$$

together with

$$\begin{aligned} \boldsymbol{\omega}_{n+1} &= \frac{2}{\Delta t} \boldsymbol{\theta} - \exp_{\mathrm{S0(3)}}\left(\widehat{\boldsymbol{\theta}}\right) \boldsymbol{\omega}_n \\ (\boldsymbol{d}_i)_{n+\alpha} &= \exp_{\mathrm{S0(3)}}\left(\alpha \widehat{\boldsymbol{\theta}}\right) (\boldsymbol{d}_i)_n \end{aligned} \tag{114}$$

for $i = 1, 2, 3$ and $\alpha \in \{1/2, 1\}$. The two algebraic equations emanating from (113) in conjunction with (114) can be used to solve for the two unknowns θ_1 and θ_2 which specify incremental rotations of the from

$$\boldsymbol{\theta} = \theta_1 (\boldsymbol{d}_1)_n + \theta_2 (\boldsymbol{d}_2)_n. \tag{115}$$

We refer to Appendix B.1 for details of the implementation.

Remark 5.2. An alternative material version of the above scheme has been proposed by Simo et al. [40, Section 4]. Let $\boldsymbol{\Lambda}$ be a rotation matrix such that $\boldsymbol{d}_i = \boldsymbol{\Lambda} \boldsymbol{e}_i$, for $i = 1, 2, 3$, and introduce the material (or convective) vectors

$$\boldsymbol{\Theta} = \boldsymbol{\Lambda}_n^T \boldsymbol{\theta}, \quad \boldsymbol{\Omega}_n = \boldsymbol{\Lambda}_n^T \boldsymbol{\omega}_n, \quad \boldsymbol{\Omega}_{n+1} = \boldsymbol{\Lambda}_{n+1}^T \boldsymbol{\omega}_{n+1}. \tag{116}$$

The scheme proposed in [40, Section 4] reads

$$\begin{aligned} &\boldsymbol{\Theta} = \frac{\Delta t}{2} [\boldsymbol{\Omega}_n + \boldsymbol{\Omega}_{n+1}], \\ &\boldsymbol{\Lambda}_{n+\alpha} = \boldsymbol{\Lambda}_n \exp_{\mathrm{S0(3)}}\left(\alpha \widehat{\boldsymbol{\Theta}}\right), \\ &\bar{I}_\varrho [\boldsymbol{\Lambda}_{n+1} \boldsymbol{\Omega}_{n+1} - \boldsymbol{\Lambda}_n \boldsymbol{\Omega}_n] = -\Delta t \boldsymbol{\Lambda}_{n+\frac{1}{2}} \boldsymbol{e}_3 \times \nabla_d \overline{V}|_{n+\frac{1}{2}}. \end{aligned} \tag{117}$$

It can be easily verified by using (116), that the Eq. $(117)_{1,2}$ are equivalent to those in (114). Moreover, scalar multiplying $(117)_3$ by $\boldsymbol{d}_{n+\frac{1}{2}}$ yields (see [40, Proposition 4.1] for details)

$$\boldsymbol{d}_{n+\frac{1}{2}} \cdot [\boldsymbol{\Lambda}_{n+1} \boldsymbol{\Omega}_{n+1} - \boldsymbol{\Lambda}_n \boldsymbol{\Omega}_n] = 0. \tag{118}$$

With regard to (116), the last equation is equivalent to the identity $(\boldsymbol{\omega}_{n+1} - \boldsymbol{\omega}_n) \cdot \boldsymbol{d}_{n+\frac{1}{2}} = 0$ (cf. [38, Appendix]). Property (118) implies that $\boldsymbol{\Omega}_n \cdot \boldsymbol{e}_3 = 0$ and $\boldsymbol{\Omega}_{n+1} \cdot \boldsymbol{e}_3 = 0$, so that, with regard to $(117)_1$, $\boldsymbol{\Theta} \cdot \boldsymbol{e}_3 = 0$. These properties make possible the reduction of the rotational dynamics to a two degrees of freedom problem. Accordingly, the vectors $\boldsymbol{\Omega}_n$, $\boldsymbol{\Omega}_{n+1}$ and $\boldsymbol{\Theta}$ can be expressed in terms of two components lying in the $\boldsymbol{e}_1, \boldsymbol{e}_2$ plane. This is consistent with expressions (103) and (115) for the spatial quantities $\boldsymbol{\omega}$ and $\boldsymbol{\theta}$. The projection of $(117)_3$ onto the plane spanned by $(\boldsymbol{d}_1)_{n+\frac{1}{2}}$ and $(\boldsymbol{d}_2)_{n+\frac{1}{2}}$ yields two equations which are equivalent to (113).

With regard to Remark 5.1, Eq. $(117)_3$ can be identified as conservation form of the mid-point rule. Consequently, $(117)_3$ can also be written in the form

$$\bar{\boldsymbol{J}}_{\varphi n+1} - \bar{\boldsymbol{J}}_{\varphi n} = -\Delta t \boldsymbol{d}_{n+\frac{1}{2}} \times \nabla_d \overline{V}|_{n+\frac{1}{2}}, \tag{119}$$

where expression (110) for the spin angular momentum has been used. The last equation automatically facilitates conservation of angular momentum.

5.4. Discretization of the DAEs and subsequent size-reduction

To summarize the procedure outlined above, the time discretization of the rotational dynamics pertaining to the model problem under consideration can be divided into two main steps: First, the underlying DAEs have been converted to ODEs on S^2 through the size-reduction outlined in Section 5.2. Subsequently, in Section 5.3, the ODEs on S^2 have been discretized to obtain a momentum conserving scheme.

We next present an alternative procedure which is advocated in the present work and has been developed in [5] for general constrained mechanical systems. In essence, the proposed approach relies on reversing the order of the two main steps summarized above. That is, we first discretize the DAEs and then perform a size-reduction of the discrete system. Note that the two alternative procedures do not commute since the manifold of interest, namely S^2, is nonlinear.

We apply the time discretization outlined in Section 4.1 to the present DAEs $(92)_{2,3}$ governing the rotational motion of the dumbbell. Accordingly, in the present context, the BEM scheme (66) assumes the form

$$\begin{aligned}
&\boldsymbol{d}_{n+1}-\boldsymbol{d}_n=\frac{\Delta t}{2}\left[\boldsymbol{v}_n^d+\boldsymbol{v}_{n+1}^d\right],\\
&\bar{I}_\varrho\left[\boldsymbol{v}_{n+1}^d-\boldsymbol{v}_n^d\right]=-\Delta t\left[\bar{\nabla}_d V+\lambda_{n+1}\boldsymbol{d}_{n+\frac{1}{2}}\right],\\
&0=\frac{1}{2}\left(\|\boldsymbol{d}_{n+1}\|^2-1\right).
\end{aligned}\tag{120}$$

Inserting from $(120)_1$ into $(120)_2$ yields

$$\frac{2\bar{I}_\varrho}{\Delta t}(\boldsymbol{d}_{n+1}-\boldsymbol{d}_n)-2\bar{I}_\varrho\,\boldsymbol{v}_n^d+\Delta t\left(\bar{\nabla}_d V+\lambda_{n+1}\boldsymbol{d}_{n+\frac{1}{2}}\right)=\boldsymbol{0}.\tag{121}$$

The last equation together with $(120)_3$ can be used to solve for $\boldsymbol{d}_{n+1}$ and λ_{n+1}. For further details, see Appendix B.2.1. Alternatively, we may apply the discrete size-reduction procedure outlined in Section 4.2 to obtain the REM scheme. To this end, we introduce a discrete version of the null space matrix (107). Similar to the continuous case the discrete null space matrix serves the purpose of (i) eliminating the discrete constraint forces, and (ii) reducing the size of the system. As discrete null space matrix we choose

$$\widetilde{\boldsymbol{\Lambda}}=\left[\begin{array}{cc}\widetilde{\boldsymbol{d}}_1 & \widetilde{\boldsymbol{d}}_2\end{array}\right]\tag{122}$$

with

$$\widetilde{\boldsymbol{d}}_\alpha=(\boldsymbol{d}_\alpha)_n-\frac{(\boldsymbol{d}_\alpha)_n\cdot\boldsymbol{d}_{n+\frac{1}{2}}}{\boldsymbol{d}_n\cdot\boldsymbol{d}_{n+\frac{1}{2}}}\boldsymbol{d}_n\tag{123}$$

for $\alpha=1,2$. In addition to that, we aim at a mapping of the form (74). For this purpose we introduce two coordinates $\theta_1,\theta_2\in\mathbb{R}$ for the parametrization of S^2. These coordinates play the role of new unknowns for the specification of the incremental rotation through the relationship

$$(\boldsymbol{d}_i)_{n+1}=\exp_{SO(3)}\left(\theta_1(\widehat{\boldsymbol{d}_1})_n+\theta_2(\widehat{\boldsymbol{d}_2})_n\right)(\boldsymbol{d}_i)_n\tag{124}$$

for $i=1,2,3$. Note that the inextensibility constraint $(120)_3$ of the original scheme is identically fulfilled by the reparametrization (124). To summarize, the resulting REM scheme provides two algebraic equations of the form

$$\left[\begin{array}{cc}\widetilde{\boldsymbol{d}}_1 & \widetilde{\boldsymbol{d}}_2\end{array}\right]^T\widetilde{\boldsymbol{R}}=\boldsymbol{0}\quad\text{with}\quad\widetilde{\boldsymbol{R}}=\frac{2\bar{I}_\varrho}{\Delta t}(\boldsymbol{d}_{n+1}-\boldsymbol{d}_n)-2\bar{I}_\varrho\,\boldsymbol{v}_n^d+\Delta t\bar{\nabla}_d V,\tag{125}$$

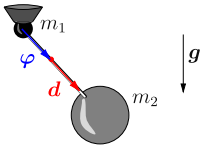

Fig. 5. The pendulum.

which can be used to determine the unknowns θ_1,θ_2. For further details of the implementation, see Appendix B.2.2.

Remark 5.3. Concerning the design of valid discrete null space matrices one may choose any 3×2 matrix $[\bar{\boldsymbol{d}}_1,\bar{\boldsymbol{d}}_2]$ with linearly independent column vectors for which the relationship $\bar{\boldsymbol{d}}_\alpha\cdot\boldsymbol{d}_{n+\frac{1}{2}}=0$ $(\alpha=1,2)$ is satisfied. For example, as an alternative to (122), one may set up a rotation matrix $\boldsymbol{\Lambda}$ which maps $\boldsymbol{e}_3=[\,0\quad 0\quad 1\,]$ to $\boldsymbol{d}_{n+\frac{1}{2}}/\|\boldsymbol{d}_{n+\frac{1}{2}}\|$. Then set $\bar{\boldsymbol{d}}_\alpha=\boldsymbol{\Lambda}\boldsymbol{e}_\alpha$ which obviously satisfies $\bar{\boldsymbol{d}}_\alpha\cdot\boldsymbol{d}_{n+\frac{1}{2}}=\|\boldsymbol{d}_{n+\frac{1}{2}}\|\boldsymbol{e}_\alpha\cdot\boldsymbol{\Lambda}^T\boldsymbol{\Lambda}\boldsymbol{e}_3=\|\boldsymbol{d}_{n+\frac{1}{2}}\|\boldsymbol{e}_\alpha\cdot\boldsymbol{e}_3=0$ for $\alpha=1,2$. This approach has been used in Simo and Tarnow [39, cf. Remark 10 (3)]. A similar ad-hoc construction can be found in Brank et al. [15, Box 1].

5.5. Incorporation of external constraints

We next demonstrate the incorporation of external constraints of the form (29). In particular, we consider the dumbbell with mass m_1 fixed, leading to the pendulum depicted in Fig. 5. The associated constraint equation can be written in the form

$$\overline{\boldsymbol{\Phi}}_{\text{ext}}(\boldsymbol{q})=\overline{\boldsymbol{G}}_{\text{ext}}\boldsymbol{q}=\boldsymbol{0}\tag{126}$$

with

$$\overline{\boldsymbol{G}}_{\text{ext}}=[\,\boldsymbol{I}_3\quad-\xi_1\boldsymbol{I}_3\,],\quad\boldsymbol{q}=\begin{bmatrix}\boldsymbol{\varphi}\\ \boldsymbol{d}\end{bmatrix}\quad\text{and}\quad\xi_1=\frac{m_2}{\bar{A}_\varrho}h.\tag{127}$$

The motion of the pendulum is characterized by the following formulation: find $\boldsymbol{q}\in\mathbb{R}^6$ and $\boldsymbol{\lambda}\in\mathbb{R}^4$ such that

$$\begin{aligned}
&\overline{\boldsymbol{M}}\ddot{\boldsymbol{q}}+\nabla_q\overline{V}+\overline{\boldsymbol{G}}^T\boldsymbol{\lambda}=\boldsymbol{0},\\
&\overline{\boldsymbol{G}}_{\text{ext}}\boldsymbol{q}=\boldsymbol{0},\\
&\overline{\Phi}_{\text{int}}(\boldsymbol{q})=0.
\end{aligned}\tag{128}$$

Here, the mass matrix $\overline{\boldsymbol{M}}$ and the constraint matrix $\overline{\boldsymbol{G}}$ are given by

$$\overline{\boldsymbol{M}}=\begin{bmatrix}\bar{A}_\varrho\boldsymbol{I} & \boldsymbol{0}\\ \boldsymbol{0} & \bar{I}_\varrho\boldsymbol{I}\end{bmatrix}\quad\text{and}\quad\overline{\boldsymbol{G}}=\begin{bmatrix}\overline{\boldsymbol{G}}_{\text{int}}\\ \overline{\boldsymbol{G}}_{\text{ext}}\end{bmatrix}=\begin{bmatrix}\boldsymbol{0}^T & \boldsymbol{d}^T\\ \boldsymbol{I}_3 & -\xi_1\boldsymbol{I}_3\end{bmatrix},\tag{129}$$

respectively. Note that the DAEs (128) have the same structure as the DAEs (46) governing the motion of semi-discrete shells. In particular, the algebraic constraints restrict possible configurations to Q_1, where Q_1 is given by (31) with node = 1. Moreover, admissible velocities $\dot{\boldsymbol{q}}\in T_qQ_1$ can be written in the form

$$\dot{\boldsymbol{q}}=\overline{\boldsymbol{P}}\boldsymbol{V}\quad\text{with}\quad\overline{\boldsymbol{P}}=\begin{bmatrix}\xi_1\overline{\boldsymbol{\Lambda}}\\ \overline{\boldsymbol{\Lambda}}\end{bmatrix}.\tag{130}$$

In this connection, the 3×2 matrix $\overline{\boldsymbol{\Lambda}}$ is given by (107). By design, the null space matrix $\overline{\boldsymbol{P}}$ has the following properties: (i) $\overline{\boldsymbol{P}}$ has full column rank, and (ii) $\overline{\boldsymbol{G}}\overline{\boldsymbol{P}}=\boldsymbol{0}$.

Remark 5.4. Explicit expressions for the null space matrix can be systematically generated through a velocity analysis which takes into account the algebraic constraints on the velocity level, such that the conditions $\overline{\boldsymbol{G}}_{\text{int}}\dot{\boldsymbol{q}}=\boldsymbol{0}$ and $\overline{\boldsymbol{G}}_{\text{ext}}\dot{\boldsymbol{q}}=\boldsymbol{0}$ are satisfied. If first the external constraints are considered, and second the internal ones we obtain

$$\overline{\boldsymbol{P}}=\overline{\boldsymbol{P}}^a_{\text{ext}}\overline{\boldsymbol{P}}^b_{\text{int}}\quad\text{with}\ \overline{\boldsymbol{P}}^a_{\text{ext}}=\begin{bmatrix}\xi_1\boldsymbol{I}\\ \boldsymbol{I}\end{bmatrix}\quad\text{and}\quad\overline{\boldsymbol{P}}^b_{\text{int}}=\overline{\boldsymbol{\Lambda}}.\tag{131}$$

Obviously, $\overline{\boldsymbol{G}}_{\text{ext}}\overline{\boldsymbol{P}}^a_{\text{ext}} = \boldsymbol{0}$, as well as $\overline{\boldsymbol{G}}_{\text{int}}\overline{\boldsymbol{P}} = \boldsymbol{0}$. In particular, velocities $\dot{\boldsymbol{q}} \in T_q\mathrm{Q}_1$ can be written in the form

$$\dot{\boldsymbol{q}} = \overline{\boldsymbol{P}}^a_{\text{ext}}\dot{\boldsymbol{d}} \tag{132}$$

for $\dot{\boldsymbol{d}} \in T_d\mathrm{S}^2$. If one proceeds the other way round one obtains

$$\overline{\boldsymbol{P}} = \overline{\boldsymbol{P}}^a_{\text{int}}\overline{\boldsymbol{P}}^b_{\text{ext}} \quad \text{with } \overline{\boldsymbol{P}}^a_{\text{int}} = \begin{bmatrix} \boldsymbol{I}_3 & \boldsymbol{0}_{3\times 2} \\ \boldsymbol{0}_{3\times 3} & \overline{\boldsymbol{\Lambda}} \end{bmatrix} \quad \text{and} \quad \overline{\boldsymbol{P}}^b_{\text{ext}} = \begin{bmatrix} \xi_1\overline{\boldsymbol{\Lambda}} \\ \boldsymbol{I}_2 \end{bmatrix}. \tag{133}$$

Now $\overline{\boldsymbol{G}}_{\text{int}}\overline{\boldsymbol{P}}^a_{\text{int}} = \boldsymbol{0}$, and $\overline{\boldsymbol{G}}_{\text{ext}}\overline{\boldsymbol{P}} = \boldsymbol{0}$. We refer to Betsch and Leyendecker [7] and Betsch and Uhlar [12] for further details about the systematic design of null space matrices for lower kinematic pairs and closed-loop multibody systems.

We next perform a size-reduction of the DAEs (128) along the lines of Section 5.2. Pre-multiplying $(128)_1$ by $\overline{\boldsymbol{P}}^T$ completely eliminates the constraint forces and reduces the number of equations from six to two. Accordingly,

$$\overline{\boldsymbol{\Lambda}}^T\left[\overline{\boldsymbol{P}}^{a^T}_{\text{ext}}\overline{\boldsymbol{M}}\overline{\boldsymbol{P}}^a_{\text{ext}}\ddot{\boldsymbol{d}} + \overline{\boldsymbol{P}}^{a^T}_{\text{ext}}\nabla_q\overline{V}\right] = \boldsymbol{0}. \tag{134}$$

A straightforward calculation yields

$$\begin{aligned} \overline{\boldsymbol{P}}^{a^T}_{\text{ext}}\overline{\boldsymbol{M}}\overline{\boldsymbol{P}}^a_{\text{ext}} &= m_2h^2 =: \overline{I}^0_{\varrho} \\ \overline{\boldsymbol{P}}^{a^T}_{\text{ext}}\nabla_q\overline{V} &= \xi_1\nabla_{\varphi}\overline{V} + \nabla_d\overline{V} =: \nabla\widetilde{V}(\boldsymbol{d}) \end{aligned} \tag{135}$$

with $\widetilde{V}(\boldsymbol{d}) = \overline{V}(\xi_1\boldsymbol{d}, \boldsymbol{d})$. Employing the above relationships together with (108), Eq. (134) yields

$$\overline{\boldsymbol{\Lambda}}^T\left[\overline{I}^0_{\varrho}\dot{\boldsymbol{\omega}} \times \boldsymbol{d} + \nabla\widetilde{V}(\boldsymbol{d})\right] = \boldsymbol{0}. \tag{136}$$

To summarize, the original DAEs (128) governing the motion of the pendulum have been converted to ODEs on S^2. Note that the ODEs again assume the form (109). Consequently, the two alternative time discretizations dealt with in Sections 5.3 and 5.4 can again be applied in a straightforward way.

5.6. Numerical examples

5.6.1. The pendulum

We next apply the above treated schemes to the pendulum (Fig. 6). We choose $m_2 = 10$ and $h = 1$. Gravity is acting on m_2 with associated potential function $\overline{V}(\boldsymbol{\varphi}, \boldsymbol{d}) = -\overline{A}_{\varrho}\boldsymbol{g}\cdot\boldsymbol{\varphi}$, where $\boldsymbol{g} = -10\boldsymbol{e}_3$ is the gravitational acceleration. Application of (135) yields the potential function

$$\widetilde{V}(\boldsymbol{d}) = -m_2h\boldsymbol{g}\cdot\boldsymbol{d}. \tag{137}$$

The initial values at time $t_0 = 0$ are given by $\boldsymbol{d}_0 = \boldsymbol{e}_1$ and $\boldsymbol{\omega}_0 = 5\boldsymbol{e}_2 + 5\boldsymbol{e}_3$.

The purely rotational motion of the present two degrees of freedom system is captured exceptionally well by the momentum conserving scheme dealt with in Section 5.3. Fig. 7 illustrates the superior accuracy of the momentum conserving scheme by depicting the 2-component of $\boldsymbol{d}(t)$, i.e. $\boldsymbol{d}(t)\cdot\boldsymbol{e}_2$, calculated with $\Delta t = 0.1$. Similar results have been obtained for the remaining two components as well as for the corresponding velocity components. The reference solution has been obtained with $\Delta t = 10^{-5}$. The energy–momentum scheme (see Section 5.4) requires $\Delta t = 0.01$ to yield results which are practically indistinguishable from the reference solution for $t \in [0, 2]$. As expected, both schemes conserve the 3-component of the angular momentum for arbitrary step-sizes.

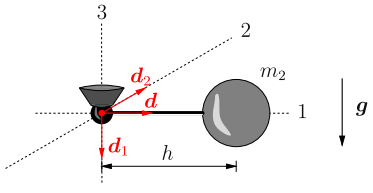

Fig. 6. Initial configuration of the pendulum.

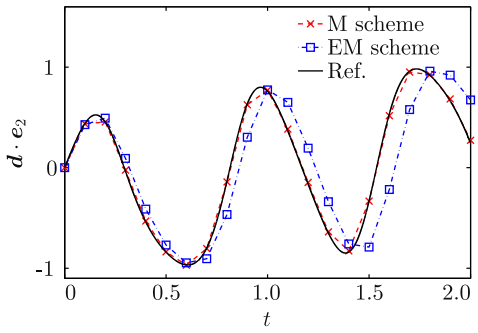

Fig. 7. Pendulum: comparison of the accuracy of the momentum (M) scheme and the energy–momentum (EM) scheme ($\Delta t = 0.1$).

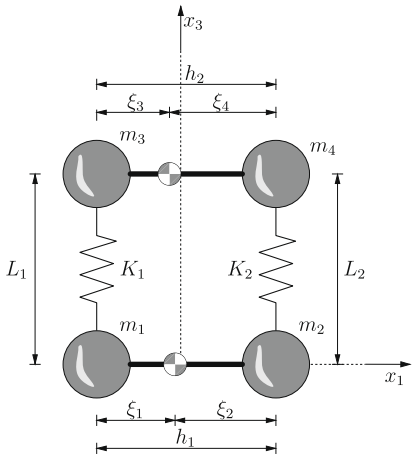

Fig. 8. Initial configuration of the spring-dumbbell system.

5.6.2. The spring-dumbbell system

In this example, we consider two dumbbells connected with two nonlinear springs as depicted in Fig. 8. Due to the presence of the springs the rotational motion is coupled to the translational one. The spring-dumbbell system can be regarded as simple model problem for nonlinear shells.

The configuration of each dumbbell is described by its center of mass $\boldsymbol{\varphi}_\alpha \in \mathbb{R}^3$ and director $\boldsymbol{d}_\alpha \in \mathrm{S}^2$ ($\alpha = 1, 2$). The potential of the springs can be written as $V_{\text{int}} = V_{\text{int},1} + V_{\text{int},2}$, where

$$V_{\text{int},\alpha} = \frac{1}{2}K_\alpha\varepsilon_\alpha^2 \quad \text{with } \varepsilon_\alpha = \frac{1}{2}\left[\left(\frac{l_\alpha}{L_\alpha}\right)^2 - 1\right]. \tag{138}$$

Here, the current spring lengths are given by

$$\begin{aligned} l_1 &= \|\boldsymbol{x}_3 - \boldsymbol{x}_1\| = \|\boldsymbol{\varphi}_2 - \boldsymbol{\varphi}_1 - \xi_3\boldsymbol{d}_2 + \xi_1\boldsymbol{d}_1\|, \\ l_2 &= \|\boldsymbol{x}_4 - \boldsymbol{x}_2\| = \|\boldsymbol{\varphi}_2 - \boldsymbol{\varphi}_1 + \xi_4\boldsymbol{d}_2 - \xi_2\boldsymbol{d}_1\|. \end{aligned} \tag{139}$$

The corresponding initial values are denoted by L_1 and L_2. The governing equations of the spring-dumbbell system can be either written as DAEs in the form (49) or as ODEs on $(\mathbb{R}^3 \times \mathrm{S}^2)^2$.

We again compare the two alternative discretization approaches outlined above. Accordingly, the first approach relies on the direct discretization of the DAEs and yields an energy–momentum scheme. The second approach is based on the application of

the mid-point rule to the translational part in conjunction with the discretization of the ODEs on S^2, as outlined in Section 5.3. Concerning the calculation of the algorithmic spring forces we proceed as follows: For the EM scheme we make use of the discrete gradient of V_{int} given by (cf. Section 4.1.1)

$$\bar{\nabla}_q V_{\text{int},\alpha} = \frac{K_\alpha}{2}[\varepsilon_{\alpha n} + \varepsilon_{\alpha n+1}]\nabla_{q_{n+\frac{1}{2}}}\varepsilon_\alpha, \tag{140}$$

where the gradient of the strains is evaluated in the mid-point configuration specified by $\boldsymbol{\varphi}_{\alpha n+\frac{1}{2}} \in \mathbb{R}^3$ and $\boldsymbol{d}_{\alpha n+\frac{1}{2}} \in \mathbb{R}^3$. Note that, in this connection, $(\cdot)_{n+\frac{1}{2}} = [(\cdot)_n + (\cdot)_{n+1}]/2$. On the other hand, the momentum scheme relies on the mid-point evaluation of the gradient of V_{int} following from

$$\nabla_q V_{\text{int},\alpha}\big|_{n+\frac{1}{2}} = \frac{dV_{\text{int},\alpha}}{d\varepsilon_\alpha}\nabla_q\varepsilon_\alpha\Big|_{n+\frac{1}{2}}. \tag{141}$$

In this connection, $\boldsymbol{d}_{\alpha n+\frac{1}{2}} \in S^2$ is given by $\boldsymbol{d}_{\alpha n+\frac{1}{2}} = \boldsymbol{\Lambda}_{\alpha n+\frac{1}{2}}\boldsymbol{e}_3$, cf. Section 5.3.

The data for the present example has been chosen as follows: point masses $m_i = 1$ $(i = 1,\dots,4)$, length $h_1 = 0.2$, $h_2 = 0.2$, and spring constants $K_1 = 100$, $K_2 = 1000$. The initial configuration is given by $\boldsymbol{x}_1 = -0.1\boldsymbol{e}_1$, $\boldsymbol{x}_2 = 0.1\boldsymbol{e}_1$, $\boldsymbol{x}_3 = -0.1\boldsymbol{e}_1 + 1\boldsymbol{e}_3$, and $\boldsymbol{x}_4 = 0.1\boldsymbol{e}_1 + 1\boldsymbol{e}_3$. Alternatively,

$$\boldsymbol{\varphi}_1 = \begin{bmatrix}0\\0\\0\end{bmatrix}, \quad \boldsymbol{\varphi}_2 = \begin{bmatrix}0\\0\\1\end{bmatrix}, \quad \boldsymbol{\Lambda}_1 = \boldsymbol{\Lambda}_2 = \begin{bmatrix}0&0&1\\0&1&0\\-1&0&0\end{bmatrix}. \tag{142}$$

The initial velocities are given

$$\dot{\boldsymbol{\varphi}}_1 = \begin{bmatrix}1\\0\\-1\end{bmatrix}, \quad \dot{\boldsymbol{\varphi}}_2 = \begin{bmatrix}0\\2\\3\end{bmatrix}, \quad \boldsymbol{\omega}_1 = \begin{bmatrix}0\\3\\4\end{bmatrix}, \quad \boldsymbol{\omega}_2 = \begin{bmatrix}0\\0\\2\end{bmatrix}. \tag{143}$$

To illustrate the simulated motion of the spring-dumbbell system Fig. 9 depicts snapshots at various points t_j in time, $j \in \{0,1,2,3\}$. The numerical results obtained with $\Delta t = 10^{-5}$ serve as reference solution. For $\Delta t = 0.001$ and $t \in [0,1]$, both schemes under consideration yield results which are practically indistinguishable from the reference solution. Concerning the numerical accuracy the momentum scheme does not produce favorable results anymore. This can be observed from Fig. 10, where as representative result for the

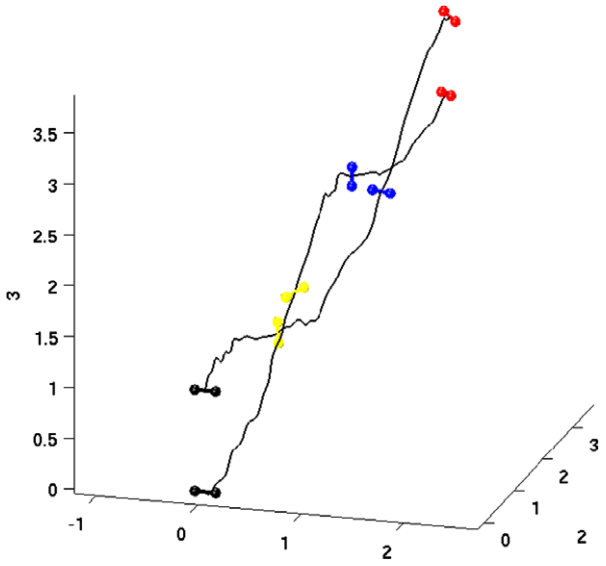

Fig. 9. Spring-dumbbell system: Snapshots of the motion at $t = 0$, $t = 1$, $t = 2$ and $t = 3$ ($\Delta t = 0.01$).

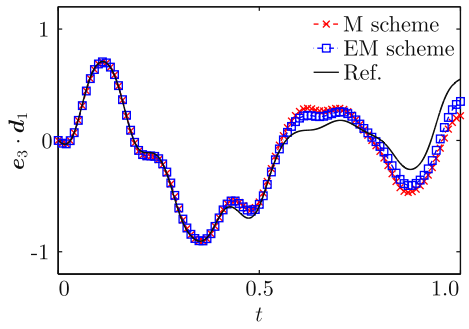

Fig. 10. Spring-dumbbell system: comparison of the accuracy of the momentum (M) scheme and the energy–momentum (EM) scheme ($\Delta t = 0.01$).

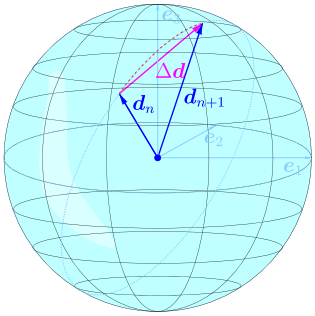

Fig. 11. Director rotations on S^2: in the advocated approach the incremental rotation of the director is characterized by the difference vector $\Delta\boldsymbol{d}$.

simulations with $\Delta t = 0.01$, the 3-component of the director $\boldsymbol{d}_1(t)$ pertaining to the first dumbbell, i.e. $\boldsymbol{e}_3 \cdot \boldsymbol{d}_1(t)$, is plotted versus time. Similar results have been obtained for the other components of both the configuration variables and the velocities.

5.7. Summary

Our numerical investigations in the context of the model problem give rise to the following conclusions. The momentum scheme resulting from the discretization of the ODEs on S^2 turned out to be tailor-made for the simulation of two degrees of freedom rotational motion. However, the favorable properties of this discretization approach vanish if the rotational motion is coupled with the translational one. This coupling is an essential feature of nonlinear shell formulations and, more generally, flexible multibody systems. Due to the coupling, methods that treat both translations and rotations on an equal footing seem to be advantageous. In the case of the dumbbell such a *uniform treatment of translations and rotations* means that rotations of the director $\boldsymbol{d} \in S^2 \subset \mathbb{R}^3$ are treated as displacements in $\mathbb{R}^3$. The unit-length constraint is only enforced at discrete points in time (see Fig. 11 for an illustration). This is in contrast to formulations relying on rotational parameters (such as that dealt with in Section 5.3) which guarantee from the outset that $\boldsymbol{d} \in S^2$.

To summarize, the salient features of the advocated approach are (i) the particular form of the DAEs which is facilitated by embedding the configuration manifold into a linear space, and (ii) the direct discretization of the DAEs. This approach entails a release from the underlying configuration manifold since the algebraic configuration constraints are only enforced at discrete points in time.

The advantages of the advocated *rotationless discretization approach* are much more pronounced in the context of nonlinear shells and flexible multibody systems. The direct discretization of the underlying DAEs yields EM schemes in a straightforward

way. In contrast to that, the use of rotational parameters within the discretization process in general leads to cumbersome expressions which severely impair the design of conserving schemes. For example, the extension to nonlinear shells of the momentum scheme outlined in Section 5.3 is not straightforward and requires a modification of the original space discretization, see Section 7.1 for further details.

6. Shells in a multibody framework

Due to the fact that the semi-discrete shell equations of motion have been cast in the form of the DAEs (49), the incorporation of smooth shells into multibody systems can be accomplished in a straightforward way. The connection of smooth shells with other bodies can be realized by adjoining additional external constraints to the underlying DAEs. In this connection, we resort to specific formulations of rigid bodies and semi-discrete beams which perfectly fit into the advocated rotationless approach (cf. Section 5.7). Moreover, folded shells can be viewed as multibody systems resulting from the assembly of smooth shells.

Consequently, the DAEs not only govern the motion of smooth semi-discrete shells but also that of folded semi-discrete shells, rigid bodies, semi-discrete beams, and flexible multibody systems in general. Concerning the time discretization of the DAEs we can still apply the approach outlined in Section 4 (see also Section 5.4) leading in a straightforward manner to a uniform energy–momentum conserving scheme for general flexible multibody systems, see also Leyendecker et al. [30].

6.1. Folded shells

We regard folded shells (or shells with intersections) as multibody system consisting of several smooth shells. For simplicity of exposition we consider in the sequel two smooth semi-discrete shells joined together leading to the model of a folded shell structure (Fig. 12). Similar to previous works by Hughes and Liu [25], Stanley et al. [41], and Simo [36] we assume that the intersections are rigid.

Consider two representative nodes A_1 and A_2 belonging to initially separate smooth shell components as depicted on the left-hand side of Fig. 12. The associated nodal configuration vectors

$$\boldsymbol{q}_{A_1} = \begin{bmatrix} \boldsymbol{\varphi}_{A_1} \\ \boldsymbol{d}_{A_1} \end{bmatrix} \quad \text{and} \quad \boldsymbol{q}_{A_2} = \begin{bmatrix} \boldsymbol{\varphi}_{A_2} \\ \boldsymbol{d}_{A_2} \end{bmatrix} \tag{144}$$

may be arranged in the vector

$$\boldsymbol{q}^{\text{Fold}} = \begin{bmatrix} \boldsymbol{q}_{A_1} \\ \boldsymbol{q}_{A_2} \end{bmatrix}. \tag{145}$$

To model the shell intersection, the two shells are joined together by imposing external nodal constraints with associated constraint function

$$\boldsymbol{\Phi}^{\text{Fold}}_{\text{ext}} = \begin{bmatrix} \boldsymbol{\varphi}_{A_2} - \boldsymbol{\varphi}_{A_1} \\ \boldsymbol{d}_{A_1} \cdot \boldsymbol{d}_{A_2} - \cos(\alpha_0) \end{bmatrix}. \tag{146}$$

Here, α_0 denotes the constant angle between $\boldsymbol{d}_{A_1}$ and $\boldsymbol{d}_{A_2}$, which has to be prescribed initially. Note that, in addition to the internal unit-length constraints, (146) specifies one more constraint on $\boldsymbol{d}_{A_1}$ and $\boldsymbol{d}_{A_2}$. Thus the six components of $\boldsymbol{d}_{A_1}$ and $\boldsymbol{d}_{A_2}$ are subject to three independent constraints leading to three rotational degrees of freedom.

6.1.1. Size-reduction

Taking into account the external constraints specified by (146), yields four additional algebraic constraints per node which can be easily appended to the DAEs (49). The discretization of the DAEs can again be performed along the lines of Section 4.1 leading to the BEM scheme.

Alternatively, as before, we may perform a size-reduction of the DAEs by eliminating the constraint forces. Guided by our previous developments we aim at a viable null space matrix $\boldsymbol{P}^{\text{Fold}}_{\text{ext}}$ which annihilates the nodal constraint forces corresponding to (146). The discrete counterpart of $\boldsymbol{P}^{\text{Fold}}_{\text{ext}}$ can then be employed in the REM scheme (see Section 4.2).

The nodal configuration vectors (145) are subject to a total of six constraints specified by

$$\boldsymbol{\Phi}^{\text{Fold}} = \begin{bmatrix} \Phi_{\text{int}_{A_1}} \\ \Phi_{\text{int}_{A_2}} \\ \boldsymbol{\Phi}^{\text{Fold}}_{\text{ext}} \end{bmatrix} \quad \text{with } \Phi_{\text{int}_{A_\alpha}} = \frac{1}{2}(\boldsymbol{d}_{A_\alpha} \cdot \boldsymbol{d}_{A_\alpha} - 1). \tag{147}$$

The corresponding 6×12 constraint Jacobian $\boldsymbol{G}^{\text{Fold}} = D\boldsymbol{\Phi}^{\text{Fold}}(\boldsymbol{q}^{\text{Fold}})$ reads

$$\boldsymbol{G}^{\text{Fold}} = \begin{bmatrix} \boldsymbol{0}^T & \boldsymbol{d}_{A_1}^T & \boldsymbol{0}^T & \boldsymbol{0}^T \\ \boldsymbol{0}^T & \boldsymbol{0}^T & \boldsymbol{0}^T & \boldsymbol{d}_{A_2}^T \\ \boldsymbol{I}_3 & \boldsymbol{0}_3 & \boldsymbol{I}_3 & \boldsymbol{0}_3 \\ \boldsymbol{0}^T & \boldsymbol{d}_{A_2}^T & \boldsymbol{0}^T & \boldsymbol{d}_{A_1}^T \end{bmatrix}. \tag{148}$$

We now aim at a null space matrix $\boldsymbol{P}^{\text{Fold}}$, which has linearly independent columns and satisfies the condition $\boldsymbol{G}^{\text{Fold}}\boldsymbol{P}^{\text{Fold}} = \boldsymbol{0}$. In particular, (cf. Remark 5.4) we make use of the multiplicative decomposition

$$\boldsymbol{P}^{\text{Fold}} = \boldsymbol{P}^{\text{Fold}}_{\text{int}}\boldsymbol{P}^{\text{Fold}}_{\text{ext}}. \tag{149}$$

Our previous treatment of the internal shell constraints completely determines the 12×10 matrix $\boldsymbol{P}^{\text{Fold}}_{\text{int}}$:

$$\boldsymbol{P}^{\text{Fold}}_{\text{int}} = \begin{bmatrix} \boldsymbol{P}_{\text{int}_{A_1}} & \boldsymbol{0} \\ \boldsymbol{0} & \boldsymbol{P}_{\text{int}_{A_2}} \end{bmatrix} \quad \text{with } \boldsymbol{P}_{\text{int}_{A_\alpha}} = \begin{bmatrix} \boldsymbol{I}_3 & \boldsymbol{0}_{3\times 2} \\ \boldsymbol{0}_3 & \overline{\boldsymbol{\Lambda}}_{A_\alpha} \end{bmatrix}. \tag{150}$$

Here, in complete analogy to the 3×2 matrix $\overline{\boldsymbol{\Lambda}}$ introduced in Section 5.2, $\overline{\boldsymbol{\Lambda}}_B$ makes possible to write nodal director velocities $\dot{\boldsymbol{d}}_B \in T_{\boldsymbol{d}_B}\mathsf{S}^2$ in the form

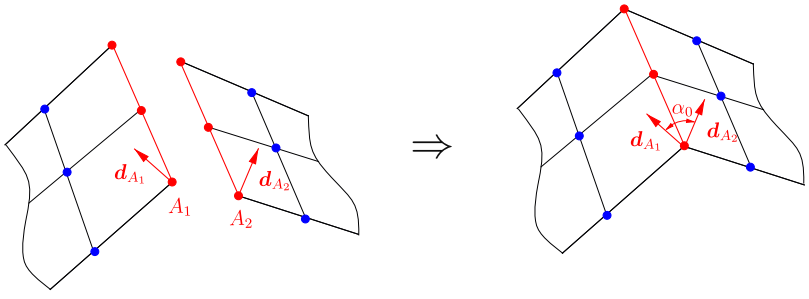

Fig. 12. Shell intersections: two smooth shell components (left) are joined together modelling a folded shell (right).

$$\dot{\boldsymbol{d}}_B = \overline{\boldsymbol{\Lambda}}_B \boldsymbol{V}_B \quad \text{with } \boldsymbol{V}_B = \begin{bmatrix} V_1 \\ V_2 \end{bmatrix}_B. \tag{151}$$

It now remains to set up matrix $\boldsymbol{P}_{\text{ext}}^{\text{Fold}}$ in (149). To this end, we link the two velocities V_1 and V_2 to the angular velocity $\boldsymbol{\omega} \in \mathbb{R}^3$, which can be associated with the three rotational degrees of freedom of the node on the intersection. Combining (106) and (107) yields the relationship

$$\boldsymbol{V} = \boldsymbol{E}\overline{\boldsymbol{\Lambda}}^T\boldsymbol{\omega} \quad \text{with } \boldsymbol{E} = \begin{bmatrix} 0 & 1 \\ -1 & 0 \end{bmatrix}. \tag{152}$$

We thus obtain the 10×6 matrix

$$\boldsymbol{P}_{\text{ext}}^{\text{Fold}} = \begin{bmatrix} \boldsymbol{P}_{\text{ext}_{A_1}} \\ \boldsymbol{P}_{\text{ext}_{A_2}} \end{bmatrix} \quad \text{with } \boldsymbol{P}_{\text{ext}_{A_\alpha}} = \begin{bmatrix} \boldsymbol{I}_3 & \boldsymbol{0}_3 \\ \boldsymbol{0}_{2\times 3} & \boldsymbol{E}\overline{\boldsymbol{\Lambda}}_{A_\alpha}^T \end{bmatrix}. \tag{153}$$

Now (149) can be calculated to obtain

$$\boldsymbol{P}^{\text{Fold}} = \begin{bmatrix} \boldsymbol{P}_{A_1}^{\text{Fold}} \\ \boldsymbol{P}_{A_2}^{\text{Fold}} \end{bmatrix} \tag{154}$$

with

$$\boldsymbol{P}_{A_\alpha}^{\text{Fold}} = \boldsymbol{P}_{\text{int}_{A_\alpha}}^{\text{Fold}} \boldsymbol{P}_{\text{ext}_{A_\alpha}}^{\text{Fold}} = \begin{bmatrix} \boldsymbol{I}_3 & \boldsymbol{0}_3 \\ \boldsymbol{0}_3 & \overline{\boldsymbol{\Lambda}}_{A_\alpha}\boldsymbol{E}\overline{\boldsymbol{\Lambda}}_{A_\alpha}^T \end{bmatrix}. \tag{155}$$

Furthermore, for each node, we obtain

$$\overline{\boldsymbol{\Lambda}}\boldsymbol{E}\overline{\boldsymbol{\Lambda}}^T = \boldsymbol{d}_1 \otimes \boldsymbol{d}_2 - \boldsymbol{d}_2 \otimes \boldsymbol{d}_1 = \boldsymbol{d}_2 \,\widehat{\times}\, \boldsymbol{d}_1 = -\widehat{\boldsymbol{d}}, \tag{156}$$

where use has been made of the fact that for $\boldsymbol{a}, \boldsymbol{b} \in \mathbb{R}^3$, $\boldsymbol{a} \otimes \boldsymbol{b} - \boldsymbol{b} \otimes \boldsymbol{a}$ is a skew-symmetric tensor with associated axial vector given by $\boldsymbol{b} \times \boldsymbol{a}$. Accordingly, combining the last two equations we eventually arrive at

$$\boldsymbol{P}_{A_\alpha}^{\text{Fold}} = \begin{bmatrix} \boldsymbol{I}_3 & \boldsymbol{0}_3 \\ \boldsymbol{0}_3 & -\widehat{\boldsymbol{d}_{A_\alpha}} \end{bmatrix}. \tag{157}$$

It can be easily verified by a direct computation that the condition $\boldsymbol{G}^{\text{Fold}}\boldsymbol{P}^{\text{Fold}} = \boldsymbol{0}$ is satisfied indeed. We further remark that result (157) is in agreement with the treatment of shell intersections in Simo [36].

Discrete setting In order to apply the REM scheme (see Section 4.2) we have to provide a discrete version of the null space matrix (149), such that the condition

$$\boldsymbol{G}^{\text{Fold}}\left(\boldsymbol{q}_{n+\frac{1}{2}}^{\text{Fold}}\right)\mathbf{P}^{\text{Fold}}\left(\boldsymbol{q}_n^{\text{Fold}}, \boldsymbol{q}_{n+1}^{\text{Fold}}\right) = \boldsymbol{0} \tag{158}$$

holds. Specifically, as discrete counterparts of (150), (153) and (157) we propose

$$\mathbf{P}_{\text{int}_{A_\alpha}} = \begin{bmatrix} \boldsymbol{I}_3 & \boldsymbol{0}_{3\times 2} \\ \boldsymbol{0}_3 & \widetilde{\boldsymbol{\Lambda}}_{A_\alpha} \end{bmatrix}, \quad \mathbf{P}_{\text{ext}_{A_\alpha}} = \begin{bmatrix} \boldsymbol{I}_3 & \boldsymbol{0}_3 \\ \boldsymbol{0}_{2\times 3} & \widetilde{\boldsymbol{E}}_{A_\alpha}\widetilde{\boldsymbol{\Lambda}}_{A_\alpha}^T \end{bmatrix}$$

$$\text{and} \quad \mathbf{P}_{A_\alpha}^{\text{Fold}} = \begin{bmatrix} \boldsymbol{I}_3 & \boldsymbol{0}_3 \\ \boldsymbol{0}_3 & -\left(\widehat{\boldsymbol{d}_{A_\alpha}}\right)_{n+\frac{1}{2}} \end{bmatrix}, \tag{159}$$

where for each node, $\widetilde{\boldsymbol{\Lambda}}_{A_\alpha}$ coincides with $\widetilde{\boldsymbol{\Lambda}}$ in (122). Moreover,

$$\widetilde{\boldsymbol{E}}_B = \begin{bmatrix} 0 & \boldsymbol{d}_{Bn} \cdot \boldsymbol{d}_{Bn+\frac{1}{2}} \\ -\boldsymbol{d}_{Bn} \cdot \boldsymbol{d}_{Bn+\frac{1}{2}} & 0 \end{bmatrix}. \tag{160}$$

That these matrices qualify indeed as discrete null space matrices can be easily verified along the lines of the continuous case treated above. In this connection, for each node, the discrete counterpart of (156) is given by

$$\widetilde{\boldsymbol{\Lambda}}\widetilde{\boldsymbol{E}}\widetilde{\boldsymbol{\Lambda}}^T = -\widehat{\boldsymbol{d}}_{n+\frac{1}{2}}. \tag{161}$$

Nodal update Within the iterative solution procedure the redundant nodal coordinates (145) can be expressed in terms of 3 incremental displacements $\boldsymbol{\mu}$ and 3 incremental rotations $\boldsymbol{\theta}$. In particular, the mapping (74) assumes the form

$$\boldsymbol{q}_{n+1}^{\text{Fold}} = \boldsymbol{F}_{q_n^{\text{Fold}}}(\boldsymbol{\mu}, \boldsymbol{\theta}), \tag{162}$$

which follows from the update formulas

$$\begin{aligned} \boldsymbol{\varphi}_{A_\alpha n+1} &= \boldsymbol{\varphi}_{A_\alpha n} + \boldsymbol{\mu}, \\ \boldsymbol{d}_{A_\alpha n+1} &= \exp_{\text{SO(3)}}(\boldsymbol{\theta})\boldsymbol{d}_{A_\alpha n}. \end{aligned} \tag{163}$$

6.2. Connection of shells to rigid bodies

We next consider the rigid connection of semi-discrete shells to rigid bodies (Fig. 13). We make use of a specific rigid body formulation which perfectly fits into the framework of the DAEs (49). We refer to Refs. [7,12] for a detailed treatment of the advocated rotationless approach to rigid body dynamics including the treatment of lower kinematic pairs.

In the underlying rigid body formulation the configuration of the rigid body is described in terms of 12 redundant coordinates which are subject to 6 independent internal constraints. Accordingly, the configuration vector of the free rigid body along with the function of internal constraints read

$$\boldsymbol{q}^R = \begin{bmatrix} \boldsymbol{\varphi}^R \\ \boldsymbol{d}_1^R \\ \boldsymbol{d}_2^R \\ \boldsymbol{d}_3^R \end{bmatrix} \quad \text{and} \quad \boldsymbol{\Phi}_{\text{int}}^R = \begin{bmatrix} [\boldsymbol{d}_1^R \cdot \boldsymbol{d}_1^R]/2 \\ [\boldsymbol{d}_2^R \cdot \boldsymbol{d}_2^R]/2 \\ [\boldsymbol{d}_3^R \cdot \boldsymbol{d}_3^R]/2 \\ \boldsymbol{d}_1^R \cdot \boldsymbol{d}_2^R \\ \boldsymbol{d}_1^R \cdot \boldsymbol{d}_3^R \\ \boldsymbol{d}_2^R \cdot \boldsymbol{d}_3^R \end{bmatrix}. \tag{164}$$

Consider a representative node B of the semi-discrete shell which is to be rigidly connected to the rigid body (Fig. 13). The nodal configuration vector and the associated internal constraint function are given by

$$\boldsymbol{q}^S = \begin{bmatrix} \boldsymbol{\varphi}_B \\ \boldsymbol{d}_B \end{bmatrix} \quad \text{and} \quad \Phi_{int_B} = \frac{1}{2}[\boldsymbol{d}_B \cdot \boldsymbol{d}_B - 1]. \tag{165}$$

Suppose that the shell director $\boldsymbol{d}_B$ does not lie in the plane spanned by $\boldsymbol{d}_1^R$ and $\boldsymbol{d}_2^R$. Then the rigid coupling is characterized by five external constraints of the form

$$\boldsymbol{\Phi}_{\text{ext}}^{SR} = \begin{bmatrix} [\boldsymbol{\varphi}_B - \boldsymbol{\varphi}^R] \cdot \boldsymbol{d}_1^R - \overline{X}^1 \\ [\boldsymbol{\varphi}_B - \boldsymbol{\varphi}^R] \cdot \boldsymbol{d}_2^R - \overline{X}^2 \\ [\boldsymbol{\varphi}_B - \boldsymbol{\varphi}^R] \cdot \boldsymbol{d}_3^R - \overline{X}^3 \\ \boldsymbol{d}_B \cdot \boldsymbol{d}_1^R - \bar{\eta}^1 \\ \boldsymbol{d}_B \cdot \boldsymbol{d}_2^R - \bar{\eta}^2 \end{bmatrix}, \tag{166}$$

where $\overline{X}^i$ and $\bar{\eta}^i = \boldsymbol{d}_B \cdot \boldsymbol{d}_i^R$ need to be specified initially. Accordingly, the 18 coordinates under consideration, namely

$$\boldsymbol{q}^{SR} = \begin{bmatrix} \boldsymbol{q}^S \\ \boldsymbol{q}^R \end{bmatrix} \tag{167}$$

are subject to 7 internal constraints plus 5 external constraints. Consequently, there remain 6 independent coordinates. For example, the nodal shell coordinates $\boldsymbol{q}^S$ can be completely expressed in terms of the coordinates of the rigid body via the relationship

$$\begin{aligned} \boldsymbol{\varphi}_B &= \boldsymbol{\varphi}^R + \overline{X}^i \boldsymbol{d}_i^R, \\ \boldsymbol{d}_B &= \bar{\eta}^i \boldsymbol{d}_i^R. \end{aligned} \tag{168}$$

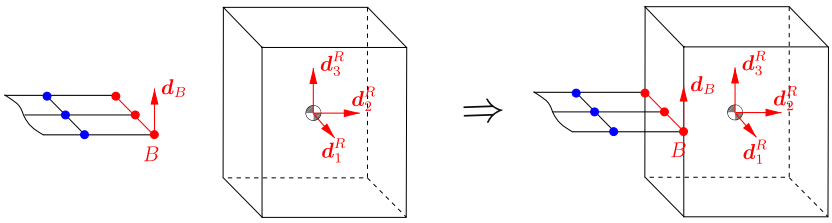

Fig. 13. Coupling of a shell with a rigid body.

The free rigid body in turn has 6 degrees of freedom. Note that (168) identically satisfies the external constraints specified by (166) and the internal constraint in (165).

6.2.1. Size-reduction

Similar to our previous developments we aim at a null space matrix $\boldsymbol{P}^{SR}$ to achieve a size-reduction of the discrete equations of motion. In particular, the time discrete version of $\boldsymbol{P}^{SR}$ is required in the REM scheme described in Section 4.2. With regard to (168), we choose the velocity $\dot{\boldsymbol{\varphi}}^R \in \mathbb{R}^3$ of the rigid body center of mass together with its angular velocity $\boldsymbol{\omega}^R \in \mathbb{R}^3$ as the six independent velocity components. Accordingly, (cf. Betsch and Leyendecker [7]) the redundant velocities of the rigid body can be written as

$$\dot{\boldsymbol{q}}^R = \boldsymbol{P}^R_{\text{int}} \begin{bmatrix} \dot{\boldsymbol{\varphi}}^R \\ \boldsymbol{\omega}^R \end{bmatrix} \quad \text{with } \boldsymbol{P}^R_{\text{int}} = \begin{bmatrix} \boldsymbol{I}_3 & \boldsymbol{0}_3 \\ \boldsymbol{0}_3 & -\widehat{\boldsymbol{d}}^R_1 \\ \boldsymbol{0}_3 & -\widehat{\boldsymbol{d}}^R_2 \\ \boldsymbol{0}_3 & -\widehat{\boldsymbol{d}}^R_3 \end{bmatrix}. \tag{169}$$

Differentiating (168) with respect to time and taking into account (169) along with (151) and (152) yields

$$\dot{\boldsymbol{q}}^S = \boldsymbol{P}^S_{\text{int}_B} \boldsymbol{P}^S_{\text{ext}_B} \begin{bmatrix} \dot{\boldsymbol{\varphi}}^R \\ \boldsymbol{\omega}^R \end{bmatrix}, \tag{170}$$

where $\boldsymbol{P}^S_{\text{int}_B}$ is given in (150), and

$$\boldsymbol{P}^S_{\text{ext}_B} = \begin{bmatrix} \boldsymbol{I}_3 & -\overline{X}^i \widehat{\boldsymbol{d}}^R_i \\ \boldsymbol{0}_{2\times 3} & \boldsymbol{E}\overline{\boldsymbol{\Lambda}}^T_B \end{bmatrix} \quad \text{so that } \boldsymbol{P}^S_{\text{int}_B} \boldsymbol{P}^S_{\text{ext}_B} = \begin{bmatrix} \boldsymbol{I}_3 & -\overline{X}^i \widehat{\boldsymbol{d}}^R_i \\ \boldsymbol{0}_3 & -\widehat{\boldsymbol{d}}_B \end{bmatrix}. \tag{171}$$

In summary, we arrive at the result

$$\dot{\boldsymbol{q}}^{SR} = \boldsymbol{P}^{SR} \begin{bmatrix} \dot{\boldsymbol{\varphi}}^R \\ \boldsymbol{\omega}^R \end{bmatrix} \quad \text{with } \boldsymbol{P}^{SR} = \begin{bmatrix} \boldsymbol{P}^S_{\text{int}_B} \boldsymbol{P}^S_{\text{ext}_B} \\ \boldsymbol{P}^R_{\text{int}} \end{bmatrix}. \tag{172}$$

Discrete setting The discrete counterpart of the null space matrix $\boldsymbol{P}^{SR}$ is given by

$$\mathbf{P}^{SR} = \begin{bmatrix} \mathbf{P}^S_{\text{int}_B} \mathbf{P}^S_{\text{ext}_B} \\ \mathbf{P}^R_{\text{int}} \end{bmatrix}. \tag{173}$$

Here, $\mathbf{P}^S_{\text{int}_B}$ is given in (159),

$$\mathbf{P}^R_{\text{int}} = \boldsymbol{P}^R_{\text{int}} \left(\boldsymbol{q}^R_{n+\frac{1}{2}} \right) \quad \text{and} \quad \mathbf{P}^S_{\text{ext}_B} = \begin{bmatrix} \boldsymbol{I}_3 & -\overline{X}^i \left(\widehat{\boldsymbol{d}}^R_i \right)_{n+\frac{1}{2}} \\ \boldsymbol{0}_{2\times 3} & \widetilde{\boldsymbol{E}}_B \widetilde{\boldsymbol{\Lambda}}^T_B \end{bmatrix}, \tag{174}$$

where again use has been made of (160). Accordingly,

$$\mathbf{P}^S_{\text{int}_B} \mathbf{P}^S_{\text{ext}_B} = \begin{bmatrix} \boldsymbol{I}_3 & -\overline{X}^i \left(\widehat{\boldsymbol{d}}^R_i \right)_{n+\frac{1}{2}} \\ \boldsymbol{0}_3 & -\left(\widehat{\boldsymbol{d}}_B \right)_{n+\frac{1}{2}} \end{bmatrix}. \tag{175}$$

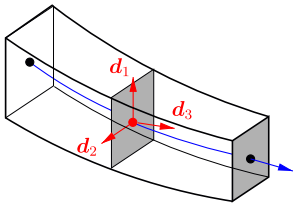

Fig. 14. Geometrically exact beam model.

Nodal update Within the iterative solution procedure the redundant coordinates (167) can be expressed in terms of 3 incremental displacements $\boldsymbol{\mu}^R$ and 3 incremental rotations $\boldsymbol{\theta}^R$ of the rigid body. In particular, the mapping (74) assumes the form

$$\boldsymbol{q}^{SR}_{n+1} = \boldsymbol{F}_{q^{SR}_n}(\boldsymbol{\mu}^R, \boldsymbol{\theta}^R), \tag{176}$$

which follows from the update formulas

$$\begin{aligned} \boldsymbol{\varphi}^R_{n+1} &= \boldsymbol{\varphi}^R_n + \boldsymbol{\mu}^R \\ \boldsymbol{d}^R_{i_{n+1}} &= \exp_{\text{SO(3)}}(\boldsymbol{\theta}^R) \boldsymbol{d}^R_{i_n} \end{aligned} \tag{177}$$

in conjunction with (168).

6.3. Incorporation of geometrically exact beams

In the present rotationless approach geometrically exact beams are treated in complete analogy to shells. We refer to Refs. [10,11,29] for further details. In short, the equations of motion pertaining to semi-discrete beams again assume the form of the DAEs in (49). Moreover, from a kinematic point of view, each node of the semi-discrete beam (Fig. 14) can be handled as a rigid body. Accordingly, the quantities in (164) can be associated with each node of the semi-discrete beam. As before, the connection between beams and other components of a multibody system can be modelled by appending further external constraints to the DAEs.

7. Numerical examples

7.1. Tumbling cylinder

We next deal with the numerical example of a (smooth) cylindrical shell that has been taken from Simo and Tarnow [39], see also Brank et al. [15]. In addition to the EM scheme emanating from our rotationless discretization approach, we consider the angular momentum conserving scheme proposed by Simo et al. [38], referred to as SRF scheme in the sequel.

The SRF scheme can be viewed as extension of the momentum conserving scheme treated in the context of the model problem (Section 5.3) to the present shell formulation. However, to retain algorithmic conservation of angular momentum, the consistent mass matrix of the semi-discrete shell formulation has to be modified by applying a specific mass lumping technique (see Appendix B.1.1 for further details).

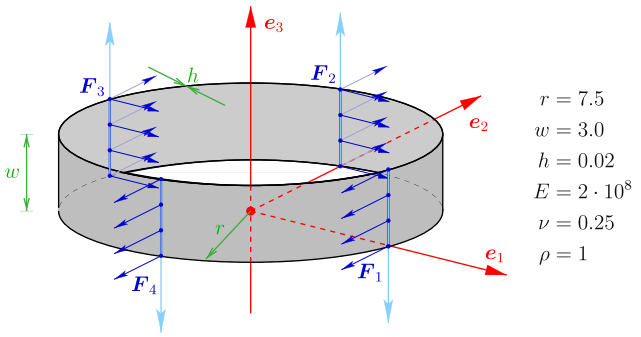

Fig. 15. Tumbling cylinder: initial configuration and external loading.

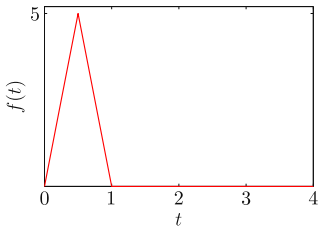

$$f(t) = \begin{cases} 10\,t & \text{for} \quad t \le 0.5 \\ 10 - 10\,t & \text{for} \quad 0.5 \le t \le 1.0 \\ 0 & \text{for} \quad t \ge 1.0 \end{cases}$$

Fig. 16. Tumbling cylinder: load function $f(t)$.

The cylinder has been discretized using 3×32 bi-linear shell elements. Starting at rest, the motion is initialized by applying external loads as depicted in Fig. 15. In particular, the nodal dead loads are given by

$$\boldsymbol{F}_i = f(t) F_i,$$

where

$$F_1 = \begin{bmatrix} 0 \\ -1 \\ -1 \end{bmatrix} \quad F_2 = \begin{bmatrix} 1 \\ 1 \\ 1 \end{bmatrix} \quad F_3 = \begin{bmatrix} 1 \\ 1 \\ 1 \end{bmatrix} \quad F_4 = \begin{bmatrix} 0 \\ -1 \\ -1 \end{bmatrix}.$$

The external loads are applied in form of a hat function over time (Fig. 16). Accordingly, for $t > 1$ no external forces act on the cylinder anymore such that the algorithmic conservation properties can be checked. To illustrate the motion a sequence of deformed shapes of the tumbling cylinder is shown in Fig. 17.

To make possible a direct comparison between the schemes SRF and EM, the mass lumping technique outlined in Appendix B.1.1 has also been applied to the EM scheme. As expected, both schemes conserve the total angular momentum (Fig. 18) independent of the step-size. Moreover, the EM scheme conserves the total energy as well. Even for the step-size $\Delta t = 0.02$ the total energy practically coincides with the reference solution obtained with $\Delta t = 10^{-4}$ (Fig. 18).

In contrast to that, the SRF scheme fails to conserve the total energy. After about 288 time steps the lack of algorithmic energy conservation eventually leads to the energy blow-up depicted in Fig. 18 ($\Delta t = 0.02$), which is accompanied by the divergence of Newton's method. On the other hand the EM scheme keeps stable (after 12,000 time steps we stopped the simulation).

Similar to the model problem dealt with in Section 5.6.2, both schemes yield almost the same solution for the nodal quantities (until the SRF scheme blows up). This can be observed from Fig. 19, in which the director component $\boldsymbol{d}_3(t) \cdot \boldsymbol{e}_3$ of the node lying initially at the position $(r, 0, 0)$ (Fig. 15) is plotted versus time.

Accordingly, compared to the present rotationless discretization approach, the use of rotational parameters in the discretization process does not pay off also in terms of accuracy. These observations add to the conclusions made in the context of the model problem (Section 5.7).

We finally remark that in the present example the BEM scheme leads to $7n_{\text{node}} = 896$ unknowns (6 redundant coordinates plus one Lagrange multiplier per node). In contrast to that, both the SRF scheme and the REM scheme yield $5n_{\text{node}} = 640$ unknowns (3 displacements plus 2 rotations per node).

7.2. Dynamics of three intersecting plates

The next example deals with three plates which are joined together as shown in Fig. 20. Two plates are discretized with

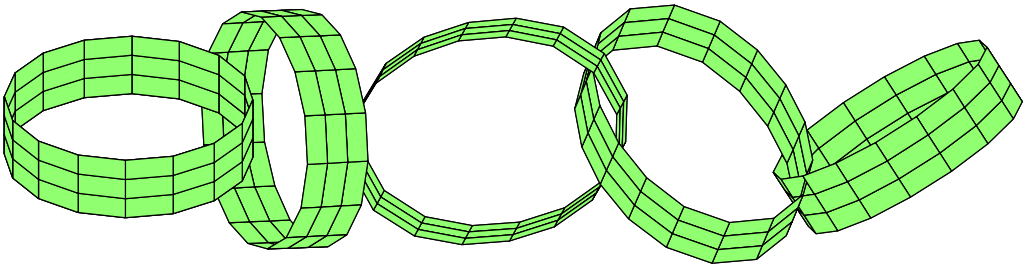

Fig. 17. Tumbling cylinder: sequence of deformed configurations.

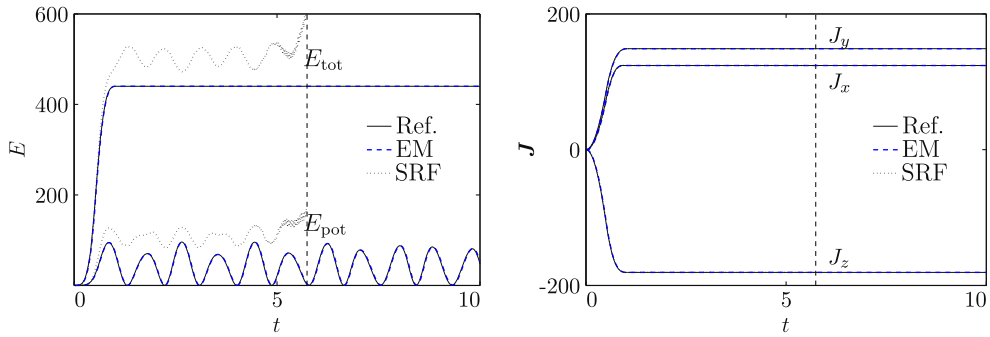

Fig. 18. Tumbling cylinder: plot of energy (left) and total angular momenta (right).

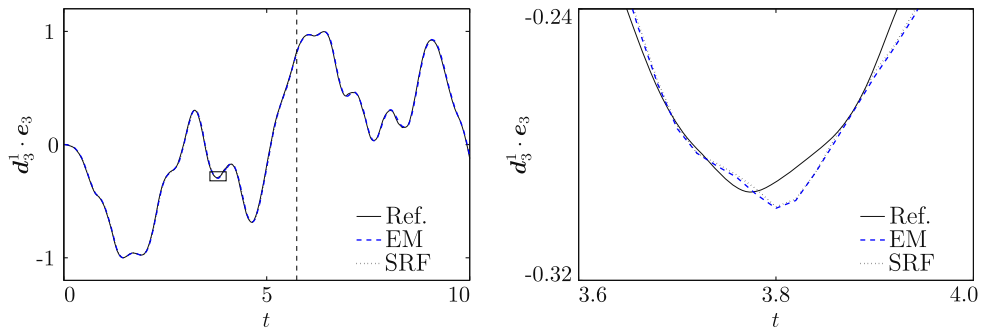

Fig. 19. Tumbling cylinder: comparison of the results for the nodal director component $\boldsymbol{d}_3(t) \cdot \boldsymbol{e}_3$.

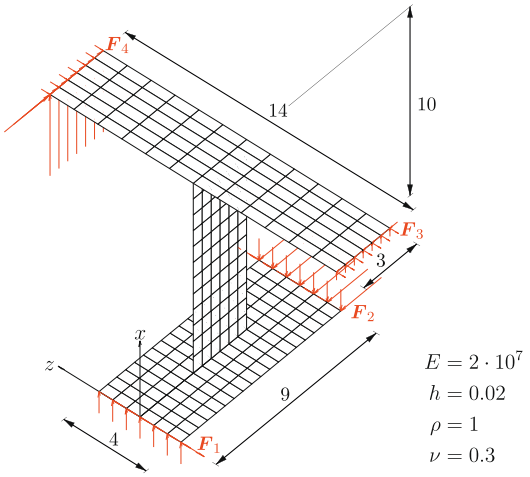

Fig. 20. Three intersecting plates: initial configuration and external loading.

6×12 bi-linear shell elements each. The third plate is discretized with 6×18 shell elements. A similar example has been investigated in Simo and Tarnow [39]. We view the present example of a folded shell as multibody system consisting of three plates, see Section 6.1 for further details.

Accordingly, in view of (146), to each node lying on an intersection we associate two directors $\boldsymbol{d}_{A_1}, \boldsymbol{d}_{A_2}$, subject to one external constraint of the form $\boldsymbol{d}_{A_1} \cdot \boldsymbol{d}_{A_2} = 0$ (in the present example $\alpha_0 = \pi/2$). The first three rows of (146) yield linear constraints which are handled by standard finite element assembly procedures.

The semi-discrete system consists of 301 nodes, where 14 nodes belong to a shell intersection. Accordingly, the underlying rotationless formulation relies on 1848 redundant coordinates subject to a total of 329 constraints. Consequently, the BEM scheme is based on 2177 unknowns, whereas the size-reduction described in Section 6.1.1 yields 1519 unknowns (which equals the number of degrees of freedom of the semi-discrete system at hand) for the REM scheme.

As indicated in Fig. 20 external nodal dead loads are applied in form of a hat function over time. In particular, the external nodal forces are given by

$$\boldsymbol{F}_i = f(t) F_i,$$

where

$$F_1 = \begin{bmatrix} 2 \\ 0 \\ -2 \end{bmatrix} \quad F_2 = \begin{bmatrix} -2 \\ -4 \\ 2 \end{bmatrix} \quad F_3 = \begin{bmatrix} 1 \\ -1 \\ -1 \end{bmatrix} \quad F_4 = \begin{bmatrix} 10 \\ 6 \\ -1 \end{bmatrix}.$$

Here, the load function assumes the form

$$f(t) = \begin{cases} 2t & \text{for } t \leqslant 0.5, \\ 2 - 2t & \text{for } 0.5 \leqslant t \leqslant 1.0, \\ 0 & \text{for } t \geqslant 1.0. \end{cases}$$

Accordingly, for $t \geqslant 1.0$ the total energy as well as the total angular momentum (and the linear momentum) are first integrals of the motion. To illustrate the resulting motion a sequence of deformed configurations is depicted in Fig. 21. It can be observed from Fig. 22 that the present EM scheme does indeed conserve total energy and angular momentum for any step-size.

7.3. Flexible multibody system – the satellite

The last example deals with the flexible multibody model of a satellite (Fig. 23). The satellite is comprised of a rigid body as well as nonlinear beam and shell components. The complete system is modelled by applying the present rotationless approach. For the space discretization a total of ten 2-node beam elements

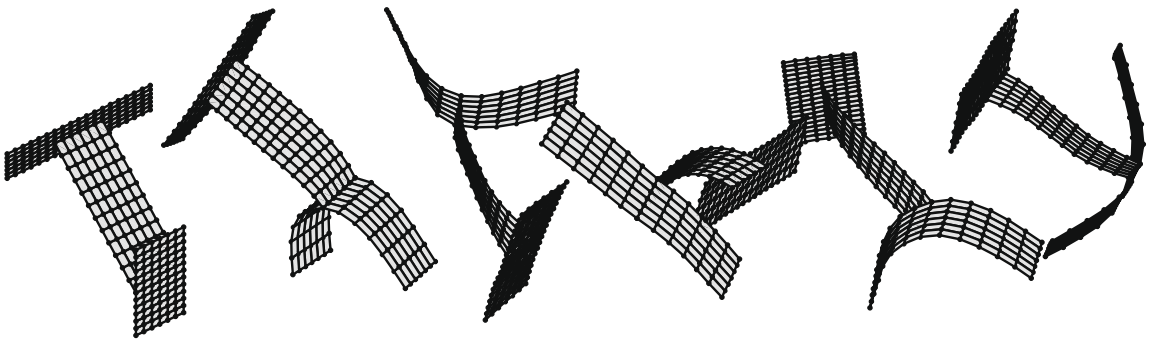

Fig. 21. Three intersecting plates: sequence of deformed configurations.

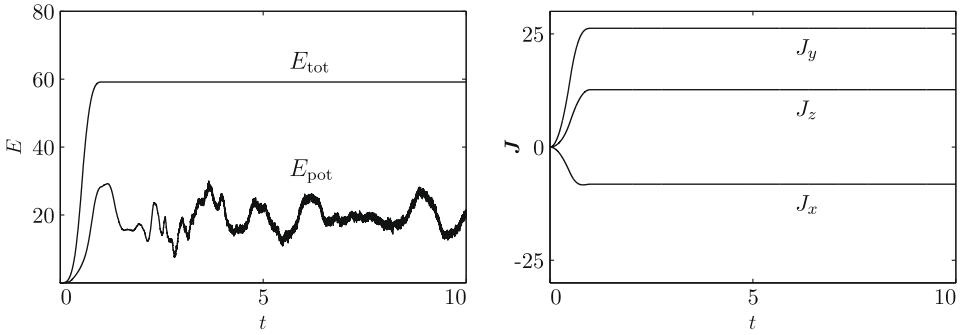

Fig. 22. Three intersecting plates: total energy and angular momentum ($\Delta t = 0.001$).

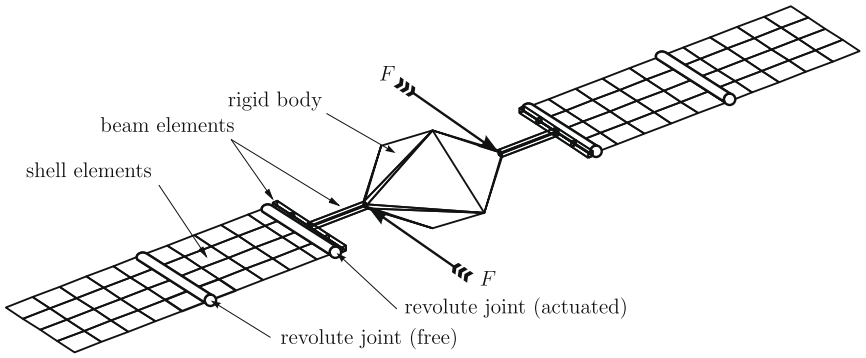

Fig. 23. The satellite: schematic of the flexible multibody system.

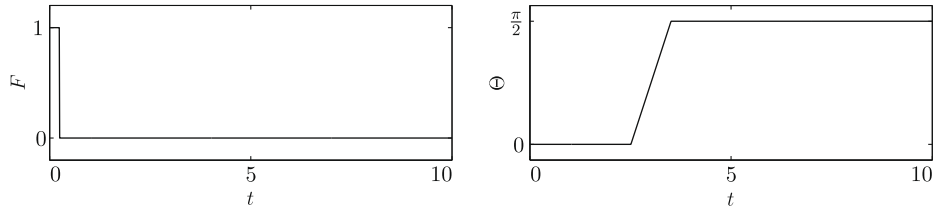

Fig. 24. The satellite: prescribed external forces (left) and actuated joint angles (right).

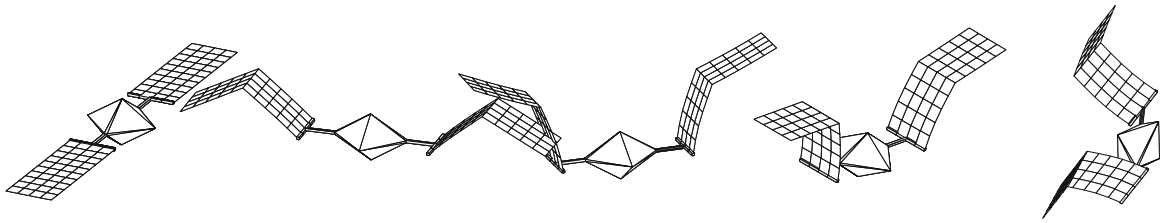

Fig. 25. The satellite: sequence of deformed configurations.

and 80 bi-linear shell elements is used. A specific coordinate augmentation technique developed in Ref. [12] is applied to actuate the revolute joints connecting the flexible panels of the satellite with its center part consisting of beams and a rigid body (cf. Fig. 23).

The discrete system gives rise to 904 redundant coordinates and 310 independent constraints. Accordingly, the implementation of the BEM scheme yields 1214 unknowns, whereas the application of the REM scheme results in a reduction to 594 unknowns.

Starting at rest, a pair of forces (Fig. 23) is applied for $t \in [0, 0.3]$ (cf. Fig. 24, left diagram). After $t = 0.3$ no external forces act on the system anymore such that the total angular momentum is a conserved quantity. For $t \in [2.5, 3.5]$ joint-torques are applied to effect the evolution of the corresponding joint-angles depicted in Fig. 24 (right diagram). This causes a motion of the panels relative to the center part of the satellite.

The simulated motion is illustrated with some snapshots of deformed configurations in Fig. 25. It can be observed from Fig. 26 that the present energy–momentum scheme correctly conserves the total energy (for $0.3 \leqslant t \leqslant 2.5$ and $t \geqslant 3.5$) as well as the total angular momentum (for $t \geqslant 0.3$). For the simulation a step-size of $\Delta t = 0.05$ has been used.

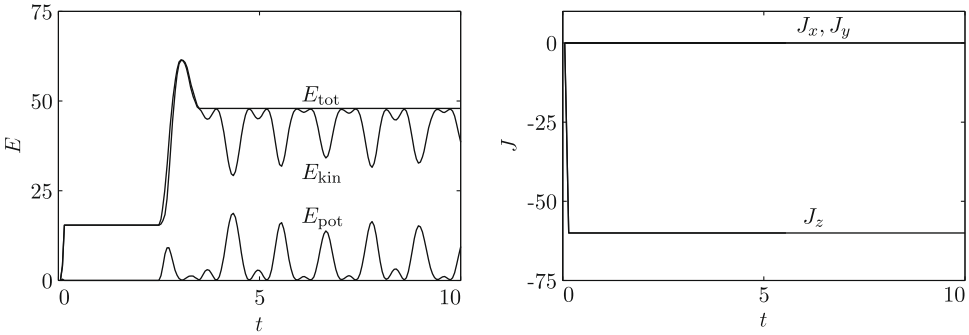

Fig. 26. The satellite: total energy and angular momentum ($\Delta t = 0.05$).

8. Conclusions

We have newly proposed a rotationless discretization in space and time of a specific geometrically exact shell model which allows a straightforward incorporation of nonlinear shells into a multibody framework. Our approach can be regarded as generalization of the work by Simo and Tarnow [39] to the realm of multibody systems.

Two alternative implementations of the proposed energy–momentum method have been presented. Details of the implementations have been described in the context of the model problem of a dumbbell (Section 5). The BEM scheme requires the solution of a generalized saddle point system in each Newton iteration. In this approach the redundant coordinates along with the Lagrange multipliers associated with the constraints are solved for simultaneously. In contrast to that, the REM scheme relies on two size-reduction steps leading to an algebraic system of equations of minimal size. In the size-reduction use is made of rotational parameters. Note, however, that the rotational parameters do not affect the underlying rotationless discretization. Although the details of both implementations are given in the context of the model problem, the extension to shells can be easily performed on a nodal basis.

The model problem served the additional purpose of comparing the present rotationless approach to more common methods relying on rotational parameters. These methods are usually based on the discretization of ODEs on a manifold. Our investigations have shown that the present rotationless approach has the following advantages over methods relying on rotational parameters:

- The equations governing the motion of rigid bodies, semi-discrete beams and shells are provided by the uniform set of DAEs (49). Accordingly, the DAEs can be used to describe the motion of general flexible multibody systems.
- The uniform DAE description of flexible multibody dynamics makes possible the application of a single time integrator. To the best of our knowledge the present approach led to the first energy–momentum scheme for arbitrary flexible multibody systems containing nonlinear shells.
- A characteristic feature of the discrete systems considered in this work is the intrinsic coupling of translational and rotational motion. Our numerical investigations presented in the context of the model problem (Section 5.6.2) and for the dynamics of smooth shells (Section 5.6.2) indicate that the use of rotations in the discretization process is not of benefit to the present systems. In contrast to that, the present rotationless approach entails a uniform treatment of both translations and rotations leading to the advantages summarized in the above two items.

Acknowledgements

Support for this research was provided by the Deutsche Forschungsgemeinschaft (DFG) under Grant BE 2285/5. This support is gratefully acknowledged.

Appendix A. General hyperelastic constitutive models

For general stored energy functions, the algorithmic stress resultants in (69) are defined by

$$\begin{aligned} n^{\alpha\beta} &= d_{a_{\alpha\beta}} W_{\kappa_{n+1}\gamma_{n+1}}(\boldsymbol{a}_n, \boldsymbol{a}_{n+1}) + d_{a_{\alpha\beta}} W_{\kappa_n\gamma_n}(\boldsymbol{a}_n, \boldsymbol{a}_{n+1}) \\ m^{\alpha\beta} &= d_{\kappa_{\alpha\beta}} W_{\boldsymbol{a}_n\gamma_{n+1}}(\boldsymbol{\kappa}_n, \boldsymbol{\kappa}_{n+1}) + d_{\kappa_{\alpha\beta}} W_{\boldsymbol{a}_{n+1}\gamma_n}(\boldsymbol{\kappa}_n, \boldsymbol{\kappa}_{n+1}) \\ q^{\beta} &= \frac{1}{2}\left[d_{\gamma_\beta} W_{\boldsymbol{a}_n\boldsymbol{\kappa}_n}(\gamma_n, \gamma_{n+1}) + \mathrm{d}_{\gamma_\beta} W_{\boldsymbol{a}_{n+1}\boldsymbol{\kappa}_{n+1}}(\gamma_n, \gamma_{n+1}) \right] \end{aligned} \tag{A.1}$$

with

$$\begin{aligned} d_{a_{\alpha\beta}} W_{\boldsymbol{\kappa}\gamma}(\boldsymbol{a}_n, \boldsymbol{a}_{n+1}) &= \frac{\partial \widetilde{W}}{\partial a_{\alpha\beta}}\left(\boldsymbol{a}_{n+\frac{1}{2}}, \boldsymbol{\kappa}, \gamma\right) \\ &\quad + \frac{\widetilde{W}(\boldsymbol{a}_{n+1}, \boldsymbol{\kappa}, \gamma) - \widetilde{W}(\boldsymbol{a}_n, \boldsymbol{\kappa}, \gamma) - \frac{\partial \widetilde{W}}{\partial a_{\nu\varrho}}(\boldsymbol{a}_{n+\frac{1}{2}}, \boldsymbol{\kappa}, \gamma)\Delta a_{\nu\varrho}}{\Delta a_{\nu\varrho}\Delta a_{\nu\varrho}} \Delta a_{\alpha\beta}, \\ d_{\kappa_{\alpha\beta}} W_{\boldsymbol{a}\gamma}(\boldsymbol{\kappa}_n, \boldsymbol{\kappa}_{n+1}) &= \frac{\partial \widetilde{W}}{\partial \kappa_{\alpha\beta}}\left(\boldsymbol{a}, \boldsymbol{\kappa}_{n+\frac{1}{2}}, \gamma\right) \\ &\quad + \frac{\widetilde{W}(\boldsymbol{a}, \boldsymbol{\kappa}_{n+1}, \gamma) - \widetilde{W}(\boldsymbol{a}, \boldsymbol{\kappa}_n, \gamma) - \frac{\partial \widetilde{W}}{\partial \kappa_{\nu\varrho}}(\boldsymbol{a}, \boldsymbol{\kappa}_{n+\frac{1}{2}}, \gamma)\Delta \kappa_{\nu\varrho}}{\Delta \kappa_{\nu\varrho}\Delta \kappa_{\nu\varrho}} \Delta \kappa_{\alpha\beta}, \\ d_{\gamma_\beta} W_{\boldsymbol{a}\boldsymbol{\kappa}}(\gamma_n, \gamma_{n+1}) &= \frac{\partial \widetilde{W}}{\partial \gamma_\beta}\left(\boldsymbol{a}, \boldsymbol{\kappa}, \gamma_{n+\frac{1}{2}}\right) \\ &\quad + \frac{\widetilde{W}(\boldsymbol{a}, \boldsymbol{\kappa}, \gamma_{n+1}) - \widetilde{W}(\boldsymbol{a}, \boldsymbol{\kappa}, \gamma_n) - \frac{\partial \widetilde{W}}{\partial \gamma_\nu}(\boldsymbol{a}, \boldsymbol{\kappa}, \gamma_{n+\frac{1}{2}})\Delta \gamma_\nu}{\Delta \gamma_\varrho \Delta \gamma_\varrho} \Delta \gamma_\beta, \end{aligned} \tag{A.2}$$

$$\Delta a_{\alpha\beta} = (a_{\alpha\beta})_{n+1} - (a_{\alpha\beta})_n, \qquad \Delta \kappa_{\alpha\beta} = (\kappa_{\alpha\beta})_{n+1} - (\kappa_{\alpha\beta})_n,$$
$$\Delta \gamma_\beta = (\gamma_\beta)_{n+1} - (\gamma_\beta)_n.$$

Appendix B. Details of the implementation

B.1. Angular momentum conserving scheme

We next consider the linearization of the residual vector pertaining to the angular momentum conserving scheme dealt with in Section 5.3. In view of (113), Newton's method requires the linearization of

$$R(\boldsymbol{\theta}) = \left[(\boldsymbol{d}_1)_{n+\frac{1}{2}} \quad (\boldsymbol{d}_2)_{n+\frac{1}{2}} \right]^T \left(\bar{I}_\varrho(\boldsymbol{\omega}_{n+1} - \boldsymbol{\omega}_n) \times \boldsymbol{d}_{n+\frac{1}{2}} + \Delta t \nabla_d V|_{n+\frac{1}{2}} \right). \tag{B.1}$$

To this end, we first linearize $(114)_2$, leading to

$$\begin{aligned}
\Delta(\boldsymbol{d}_i)_{n+\alpha} &= \frac{\mathrm{d}}{\mathrm{d}\varepsilon}\Big|_{\varepsilon=0} \exp\Big(\alpha(\boldsymbol{\theta}+\widehat{\varepsilon\Delta\boldsymbol{\theta}})\Big)(\boldsymbol{d}_i)_n,\\
\Delta(\boldsymbol{d}_i)_{n+\alpha} &= \frac{\mathrm{d}}{\mathrm{d}\varepsilon}\Big|_{\varepsilon=0} \exp\Big(\alpha(\boldsymbol{\theta}+\widehat{\varepsilon\Delta\boldsymbol{\theta}})\Big)\exp\Big(-\alpha\widehat{\boldsymbol{\theta}}\Big)(\boldsymbol{d}_i)_{n+\alpha},\\
\Delta(\boldsymbol{d}_i)_{n+\alpha} &= \overset{\triangle}{\boldsymbol{\omega}}(\alpha\boldsymbol{\theta})\times(\boldsymbol{d}_i)_{n+\alpha},
\end{aligned} \tag{B.2}$$

where

$$\overset{\triangle}{\boldsymbol{\omega}}(\alpha\boldsymbol{\theta}) = \boldsymbol{H}(\alpha\boldsymbol{\theta})\alpha\Delta\boldsymbol{\theta} \tag{B.3}$$

with

$$\begin{aligned}
\boldsymbol{H}(\boldsymbol{\theta}) = \frac{\sin(\|\boldsymbol{\theta}\|)}{\|\boldsymbol{\theta}\|}\boldsymbol{I} + \frac{1-\cos(\|\boldsymbol{\theta}\|)}{\|\boldsymbol{\theta}\|}\frac{\widehat{\boldsymbol{\theta}}}{\|\boldsymbol{\theta}\|}\\
+\left(1-\frac{\sin(\|\boldsymbol{\theta}\|)}{\|\boldsymbol{\theta}\|}\right)\frac{\boldsymbol{\theta}\otimes\boldsymbol{\theta}}{\|\boldsymbol{\theta}\|^2}.
\end{aligned} \tag{B.4}$$

Consequently,

$$\Big[\,(\Delta\boldsymbol{d}_1)_{n+\frac{1}{2}} \quad \Delta(\boldsymbol{d}_2)_{n+\frac{1}{2}}\,\Big]^T\boldsymbol{a} = \Big[\,(\boldsymbol{d}_1)_{n+\frac{1}{2}} \quad (\boldsymbol{d}_2)_{n+\frac{1}{2}}\,\Big]^T\widehat{\boldsymbol{a}}\,\overset{\triangle}{\boldsymbol{\omega}}(\boldsymbol{\theta}/2) \tag{B.5}$$

for any $\boldsymbol{a}\in\mathbb{R}^3$.

Secondly, with regard to $(114)_1$, we get

$$\begin{aligned}
\Delta\boldsymbol{\omega}_{n+1} &= \frac{\mathrm{d}}{\mathrm{d}\varepsilon}\Big|_{\varepsilon=0}\left(\frac{2}{\Delta t}(\boldsymbol{\theta}+\varepsilon\Delta\boldsymbol{\theta}) - \exp\Big((\boldsymbol{\theta}+\widehat{\varepsilon\Delta\boldsymbol{\theta}})\Big)\boldsymbol{\omega}_n\right)\\
\Delta\boldsymbol{\omega}_{n+1} &= \frac{2}{\Delta t}\Delta\boldsymbol{\theta} - \frac{\mathrm{d}}{\mathrm{d}\varepsilon}\Big|_{\varepsilon=0}\exp\Big((\boldsymbol{\theta}+\widehat{\varepsilon\Delta\boldsymbol{\theta}})\Big)\exp\Big(-\widehat{\boldsymbol{\theta}}\Big)\exp\Big(\widehat{\boldsymbol{\theta}}\Big)\boldsymbol{\omega}_n\\
\Delta\boldsymbol{\omega}_{n+1} &= \frac{2}{\Delta t}\Delta\boldsymbol{\theta} - \overset{\triangle}{\boldsymbol{\omega}}(\boldsymbol{\theta})\times\Big[\exp\Big(\widehat{\boldsymbol{\theta}}\Big)\boldsymbol{\omega}_n\Big]\\
\Delta\boldsymbol{\omega}_{n+1} &= \boldsymbol{G}(\boldsymbol{\theta})\Delta\boldsymbol{\theta}
\end{aligned} \tag{B.6}$$

with

$$\boldsymbol{G}(\boldsymbol{\theta}) = \frac{2}{\Delta t}\boldsymbol{I} + \left[\exp\Big(\widehat{\widehat{\boldsymbol{\theta}}}\Big)\boldsymbol{\omega}_n\right]\boldsymbol{H}(\boldsymbol{\theta}), \tag{B.7}$$

where again (B.3) has been employed. A tedious but straightforward calculation starting from (B.1), yields the tangent operator $K = \frac{\mathrm{d}}{\mathrm{d}\varepsilon}|_{\varepsilon=0}R(\boldsymbol{\theta}+\varepsilon\Delta\boldsymbol{\theta})$ in the form

$$K = \Big[\,(\boldsymbol{d}_1)_{n+\frac{1}{2}} \quad (\boldsymbol{d}_2)_{n+\frac{1}{2}}\,\Big]^T\widetilde{\boldsymbol{K}}\Big[\,(\boldsymbol{d}_1)_n \quad (\boldsymbol{d}_2)_n\,\Big] \tag{B.8}$$

with

$$\widetilde{\boldsymbol{K}} = -\bar{I}_\varrho\widehat{\boldsymbol{d}}_{n+\frac{1}{2}}\boldsymbol{G}(\boldsymbol{\theta}) - \frac{1}{2}\Big(\bar{I}_\varrho(\boldsymbol{\omega}_{n+1}-\boldsymbol{\omega}_n)\otimes\boldsymbol{d}_{n+\frac{1}{2}} - \Delta t\Big(\widehat{\nabla_d V}\Big)|_{n+\frac{1}{2}}\Big)\boldsymbol{H}(\boldsymbol{\theta}/2). \tag{B.9}$$

In this connection use has been made of the identity $(\boldsymbol{\omega}_{n+1}-\boldsymbol{\omega}_n)\cdot\boldsymbol{d}_{n+\frac{1}{2}} = 0$, see Remark 5.2. Moreover, for simplicity it has been assumed that $\nabla_d^2 V = \boldsymbol{0}$. Table 1 contains an outline of the implementation of the present algorithm within the iterative solution procedure.

B.1.1. Extension to shells

The momentum conserving scheme described above in the context of the model problem can be extended to the present semi-discrete shell formulation dealt with in Section 3. We next provide a short summary of the approach originally proposed by Simo et al. [38].

The semi-discrete shell equations of motion are viewed from the outset as ODEs on $\left(\mathbb{R}^3\times\mathrm{S}^2\right)^{n_{\mathrm{node}}}$. The time discretization is performed along the lines of the model problem treated in Section 5.3. To maintain algorithmic conservation of angular momentum a diagonalization of the (consistent) mass matrix is required. In what follows we focus on the contribution of the inertia terms to the discretized weak form (35), given by

$$G^h_{\mathrm{dyn}} = G_{\mathrm{dyn}}(\boldsymbol{\Phi}^h,\delta\boldsymbol{\Phi}^h) = \sum_{A,B=1}^{n_{\mathrm{node}}}\delta\boldsymbol{q}_A\cdot\boldsymbol{M}^{AB}\ddot{\boldsymbol{q}}_B. \tag{B.10}$$

Making use of the consistent mass matrix in (37) gives rise to the decomposition

$$G^h_{\mathrm{dyn}} = G^\varphi_{\mathrm{dyn}} + G^d_{\mathrm{dyn}} \tag{B.11}$$

with

$$G^\varphi_{\mathrm{dyn}} = \sum_{A,B=1}^{n_{\mathrm{node}}} M^{AB}_\varphi\delta\boldsymbol{\varphi}_A\cdot\ddot{\boldsymbol{\varphi}}_B \quad\text{and}\quad G^d_{\mathrm{dyn}} = \sum_{A,B=1}^{n_{\mathrm{node}}} M^{AB}_d\delta\boldsymbol{d}_A\cdot\ddot{\boldsymbol{d}}_B. \tag{B.12}$$

Now, the director part G^d_{dyn} is modified by applying the row-sum lumping technique (see Hughes [24, Chapter 7]) leading to

$$G^{d,SRF}_{\mathrm{dyn}} = \sum_{A=1}^{n_{\mathrm{node}}}\delta\boldsymbol{d}_A\cdot\widetilde{M}^A_d\ddot{\boldsymbol{d}}_A \tag{B.13}$$

with the components of the lumped mass matrix

$$\widetilde{M}^A_d = \sum_{B=1}^{n_{\mathrm{node}}} M^{AB}_d = \int_{\mathscr{S}^0} I_\varrho N^A\,\mathrm{d}\mathscr{S}. \tag{B.14}$$

Accordingly, the lumped mass matrix follows from adding the off-diagonal terms on each row to the diagonal term. Now, in complete analogy to Section 5.2, we get

$$G^{d,SRF}_{\mathrm{dyn}} = \sum_{A=1}^{n_{\mathrm{node}}}\delta\boldsymbol{d}_A\cdot\widetilde{M}^A_d\dot{\boldsymbol{\omega}}_A\times\boldsymbol{d}_A, \tag{B.15}$$

where $\delta\boldsymbol{d}_A\in T_{d_A}\mathrm{S}^2$ is implemented as before by setting up the triad $\{(\boldsymbol{d}_1)_A,(\boldsymbol{d}_2)_A,(\boldsymbol{d}_3)_A\equiv\boldsymbol{d}_A\}$ such that $\delta\boldsymbol{d}_A\in\mathrm{span}((\boldsymbol{d}_1)_A,(\boldsymbol{d}_2)_A)$, for $A=1,\ldots,n_{\mathrm{node}}$. The time discretization can be performed *on a nodal basis* as outlined in Section 5.3. That is, the discrete version of (B.13) yields the following nodal contribution to the residual vector

$$F^A_{dyn,\theta} = \Big[\,(\boldsymbol{d}_1)_{A_{n+\frac{1}{2}}} \quad (\boldsymbol{d}_2)_{A_{n+\frac{1}{2}}}\,\Big]^T\widetilde{M}^A_d\big(\boldsymbol{\omega}_{A_{n+1}}-\boldsymbol{\omega}_{A_n}\big)\times\boldsymbol{d}_{A_{n+\frac{1}{2}}}. \tag{B.16}$$

Note that, in contrast to the director part, the mid-surface part of the inertia terms is still consistent with the underlying finite element discretization in space. That is, both the SRF scheme and the EM scheme rely on identical nodal contributions to the residual

Table 1
Angular momentum conserving scheme: outline of the calculations within a single Newton iteration.

- Given: Initial quantities of the current time step $\{(\boldsymbol{d}_i)_n\}$, $\boldsymbol{\omega}_n$.
  Prescribed step-size Δt.
  Incremental rotation after l iterations
  $$\boldsymbol{\theta}^{(l)} = \theta_1^{(l)}(\boldsymbol{d}_1)_n + \theta_2^{(l)}(\boldsymbol{d}_2)_n.$$
- Calculate residual vector (B.1) and iteration matrix (B.8) by employing
  $$\boldsymbol{\omega}^{(l)}_{n+1} = \frac{2}{\Delta t}\boldsymbol{\theta}^{(l)} - \exp\Big(\widehat{\boldsymbol{\theta}}^{(l)}\Big)\boldsymbol{\omega}_n,$$
  $$(\boldsymbol{d}_i)^{(l)}_{n+\frac{1}{2}} = \exp\Big(\widehat{\boldsymbol{\theta}}^{(l)}/2\Big)(\boldsymbol{d}_i)_n.$$
- Solve
  $$K\Delta\boldsymbol{\Theta} = -R$$
  for
  $$\Delta\boldsymbol{\Theta} = [\,\Delta\theta_1 \quad \Delta\theta_2\,]^T$$
- Update incremental rotation
  $$\boldsymbol{\theta}^{(l+1)} = \Big(\theta_1^{(l)}+\Delta\theta_1\Big)(\boldsymbol{d}_1)_n + \Big(\theta_2^{(l)}+\Delta\theta_2\Big)(\boldsymbol{d}_2)_n$$

vector of the intertia terms associated with the mid-surface part. Specifically, with regard to the left-hand equation in (B.12),

$$G^{\varphi}_{\rm dyn} = \sum_{A=1}^{n_{\rm node}} \delta\boldsymbol{\varphi}_A \cdot F^A_{{\rm dyn},\varphi} \quad \text{with } F^A_{{\rm dyn},\varphi} = \sum_{B=1}^{n_{\rm node}} M^{AB}_{\varphi}\left[\boldsymbol{v}^{\varphi}_{B_{n+1}} - \boldsymbol{v}^{\varphi}_{B_n}\right]. \tag{B.17}$$

The nodal contribution to the residual vector can now be written in the form

$$R^A = F^A_{\rm dyn} + \Delta t\left[F^A_{\rm int}\left(\boldsymbol{q}_{n+\frac{1}{2}}\right) - F^A_{\rm ext}\left(t_{n+\frac{1}{2}}\right)\right], \tag{B.18}$$

where the contribution of the inertia terms is given by

$$F^A_{\rm dyn} = \begin{bmatrix} F^A_{{\rm dyn},\varphi} \\ F^A_{{\rm dyn},\vartheta} \end{bmatrix} = \begin{bmatrix} \sum_{B=1}^{n_{\rm node}} M^{AB}_{\varphi}\left[\boldsymbol{v}^{\varphi}_{B_{n+1}} - \boldsymbol{v}^{\varphi}_{B_n}\right] \\ \left[(\boldsymbol{d}_1)_{A_{n+\frac{1}{2}}} \quad (\boldsymbol{d}_2)_{A_{n+\frac{1}{2}}}\right]^T \widetilde{M}^A_d\left(\boldsymbol{\omega}_{A_{n+1}} - \boldsymbol{\omega}_{A_n}\right) \times \boldsymbol{d}_{A_{n+\frac{1}{2}}} \end{bmatrix}. \tag{B.19}$$

Furthermore,

$$F^A_{\rm int}\left(\boldsymbol{q}_{n+\frac{1}{2}}\right) - F^A_{\rm ext}\left(t_{n+\frac{1}{2}}\right) = P^{A^T}\left[\boldsymbol{F}^A_{\rm int}\left(\boldsymbol{q}_{n+\frac{1}{2}}\right) - \boldsymbol{F}^A_{\rm ext}\left(t_{n+\frac{1}{2}}\right)\right], \tag{B.20}$$

where $\boldsymbol{F}^A_{\rm int}$ and $\boldsymbol{F}^A_{\rm ext}$ have already been introduced in (39), and the 6×5 matrix P_A assumes the form

$$P_A = \begin{bmatrix} \boldsymbol{I}_3 & \boldsymbol{0}_{3\times 2} \\ \boldsymbol{0}_3 & \left[(\boldsymbol{d}_1)_{A_{n+\frac{1}{2}}} \quad (\boldsymbol{d}_2)_{A_{n+\frac{1}{2}}}\right] \end{bmatrix}. \tag{B.21}$$

The nodal contributions to the configuration vector $\boldsymbol{q}_{n+\frac{1}{2}} \in \mathrm{Q}_{\rm node}$ are given by

$$\begin{aligned} \boldsymbol{\varphi}_{A_{n+\frac{1}{2}}} &= \frac{1}{2}\left(\boldsymbol{\varphi}_{A_n} + \boldsymbol{\varphi}_{A_{n+1}}\right), \\ \boldsymbol{d}_{A_{n+\frac{1}{2}}} &= \exp\left(\widehat{\boldsymbol{\theta}}_A/2\right)\boldsymbol{d}_{A_n}. \end{aligned} \tag{B.22}$$

While the treatment of the translational part is standard, the rotational part can be handled on a nodal basis as summarized in Table 1. In this connection, the incremental nodal rotations are characterized by two rotational parameters $(\theta_1)_A$ and $(\theta_2)_A$, such that

$$\boldsymbol{\theta}_A = (\theta_1)_A(\boldsymbol{d}_1)_{A_n} + (\theta_2)_A(\boldsymbol{d}_2)_{A_n}. \tag{B.23}$$

B.2. Energy–momentum conserving scheme

B.2.1. BEM scheme

In the context of the model problem considered in Section 5.4, the BEM scheme yields the following algebraic system of nonlinear equations:

$$\begin{aligned} \boldsymbol{R}(\boldsymbol{d}_{n+1}, \lambda_{n+1}) &= \widetilde{\boldsymbol{R}}(\boldsymbol{d}_{n+1}) + \Delta t\lambda_{n+1}\boldsymbol{d}_{n+\frac{1}{2}}, \\ \Phi(\boldsymbol{d}_{n+1}) &= 0, \end{aligned} \tag{B.24}$$

where $\widetilde{\boldsymbol{R}}$ is given in (125), and $\Phi = (\boldsymbol{d}\cdot\boldsymbol{d} - 1)/2$. To solve for $\boldsymbol{d}_{n+1}$ and λ_{n+1} we apply Newton's method. Accordingly, in each iteration the following linear system in saddle point form has to be solved:

$$\begin{bmatrix} \left(\frac{2\bar{I}_\varrho}{\Delta t} + \frac{\Delta t\lambda_{n+1}}{2}\right)\boldsymbol{I}_3 & \Delta t\boldsymbol{d}^{(l)}_{n+\frac{1}{2}} \\ \boldsymbol{d}^{(l)T}_{n+1} & \boldsymbol{0} \end{bmatrix} \begin{bmatrix} \Delta\boldsymbol{d}_{n+1} \\ \Delta\lambda_{n+1} \end{bmatrix} = -\begin{bmatrix} \boldsymbol{R}\left(\boldsymbol{d}^{(l)}_{n+1}, \lambda^{(l)}_{n+1}\right) \\ \Phi(\boldsymbol{d}^{(l)}_{n+1}) \end{bmatrix}. \tag{B.25}$$

Note that, for simplicity, it has been assumed that $\nabla^2_d V = \boldsymbol{0}$.

B.2.2. REM scheme

With regard to Section 5.4, Eq. (125), the residual vector associated with the REM scheme assumes the form

$$\widetilde{R}(\boldsymbol{d}_{n+1}) = \begin{bmatrix} \widetilde{\boldsymbol{d}}_1 & \widetilde{\boldsymbol{d}}_2 \end{bmatrix}^T \widetilde{\boldsymbol{R}}. \tag{B.26}$$

Note that, in view of (124), $\boldsymbol{d}_{n+1}$ is expressed in terms of two incremental rotations θ_1 and θ_2. Thus, similar to the momentum scheme treated in Appendix B.1, the two incremental rotations are the primary unknowns to be solved for. In complete analogy to Appendix B.1, the following relationship holds:

$$\Delta\boldsymbol{d}_{n+1} = \overset{\triangle}{\boldsymbol{\omega}}(\boldsymbol{\theta}) \times \boldsymbol{d}_{n+1} = -\widehat{\boldsymbol{d}}_{n+1}\boldsymbol{H}(\boldsymbol{\theta})\Delta\boldsymbol{\theta}. \tag{B.27}$$

The linearization of (B.26) may be written in the form

$$D\widetilde{R}(\boldsymbol{d}_{n+1})\cdot\Delta\boldsymbol{d}_{n+1} = \begin{bmatrix} \Delta\widetilde{\boldsymbol{d}}_1 & \Delta\widetilde{\boldsymbol{d}}_2 \end{bmatrix}^T \widetilde{\boldsymbol{R}} + \begin{bmatrix} \widetilde{\boldsymbol{d}}_1 & \widetilde{\boldsymbol{d}}_2 \end{bmatrix}^T D\widetilde{\boldsymbol{R}}\cdot\Delta\boldsymbol{d}_{n+1}. \tag{B.28}$$

A straightforward calculation based on (123) yields

$$\Delta\widetilde{\boldsymbol{d}}_\alpha \cdot \widetilde{\boldsymbol{R}} = -\frac{\boldsymbol{d}_n\cdot\widetilde{\boldsymbol{R}}}{2\boldsymbol{d}_n\cdot\boldsymbol{d}_{n+\frac{1}{2}}}\widetilde{\boldsymbol{d}}_\alpha\cdot\Delta\boldsymbol{d}_{n+1} \tag{B.29}$$

for any $\boldsymbol{a}\in\mathbb{R}^3$. Accordingly,

$$\begin{bmatrix} \Delta\widetilde{\boldsymbol{d}}_1 & \Delta\widetilde{\boldsymbol{d}}_2 \end{bmatrix}^T \widetilde{\boldsymbol{R}} = -\frac{\boldsymbol{d}_n\cdot\widetilde{\boldsymbol{R}}}{2\boldsymbol{d}_n\cdot\boldsymbol{d}_{n+\frac{1}{2}}}\begin{bmatrix} \widetilde{\boldsymbol{d}}_1 & \widetilde{\boldsymbol{d}}_2 \end{bmatrix}^T \Delta\boldsymbol{d}_{n+1}. \tag{B.30}$$

Altogether, the pertinent tangent operator can be written as

$$\widetilde{K} = \begin{bmatrix} \widetilde{\boldsymbol{d}}_1 & \widetilde{\boldsymbol{d}}_2 \end{bmatrix}^T \widetilde{\boldsymbol{K}}\left[(\boldsymbol{d}_1)_n \quad (\boldsymbol{d}_2)_n\right] \tag{B.31}$$

with

$$\widetilde{\boldsymbol{K}} = \left(\frac{\boldsymbol{d}_n\cdot\widetilde{\boldsymbol{R}}}{2\boldsymbol{d}_n\cdot\boldsymbol{d}_{n+\frac{1}{2}}} - \frac{2\bar{I}_\varrho}{\Delta t}\right)\widehat{\boldsymbol{d}}_{n+\frac{1}{2}}\boldsymbol{H}(\boldsymbol{\theta}). \tag{B.32}$$

References

[1] S.S. Antman, Nonlinear Problems of Elasticity, second ed., Springer-Verlag, 2005.
[2] O.A. Bauchau, C.L. Bottasso, On the design of energy preserving and decaying schemes for flexible, nonlinear multi-body systems, Comput. Methods Appl. Mech. Engrg. 169 (1999) 61–79.
[3] O.A. Bauchau, J.-Y. Choi, C.L. Bottasso, On the modeling of shells in multibody dynamics, Multibody Syst. Dyn. 8 (2002) 459–489.
[4] T. Belytschko, W.K. Liu, B. Moran, Nonlinear Finite Elements for Continua and Structures, John Wiley & Sons, 2000.
[5] P. Betsch, The discrete null space method for the energy consistent integration of constrained mechanical systems. Part I: Holonomic constraints, Comput. Methods Appl. Mech. Engrg. 194 (50–52) (2005) 5159–5190.
[6] P. Betsch, C. Hesch, Energy–momentum conserving schemes for frictionless dynamic contact problems. Part I: NTS method, in: P. Wriggers, U. Nackenhorst (Eds.), IUTAM Symposium on Computational Methods in Contact Mechanics, IUTAM Bookseries, vol. 3, Springer-Verlag, 2007, pp. 77–96.
[7] P. Betsch, S. Leyendecker, The discrete null space method for the energy consistent integration of constrained mechanical systems. Part II: Multibody dynamics, Int. J. Numer. Methods Engrg. 67 (4) (2006) 499–552.
[8] P. Betsch, P. Steinmann, Conservation properties of a time FE method. Part III: Mechanical systems with holonomic constraints, Int. J. Numer. Methods Engrg. 53 (2002) 2271–2304.
[9] P. Betsch, P. Steinmann, A DAE approach to flexible multibody dynamics, Multibody Syst. Dyn. 8 (2002) 367–391.
[10] P. Betsch, P. Steinmann, Frame-indifferent beam finite elements based upon the geometrically exact beam theory, Int. J. Numer. Methods Engrg. 54 (2002) 1775–1788.
[11] P. Betsch, P. Steinmann, Constrained dynamics of geometrically exact beams, Comput. Mech. 31 (2003) 49–59.
[12] P. Betsch, S. Uhlar, Energy–momentum conserving integration of multibody dynamics, Multibody Syst. Dyn. 17 (4) (2007) 243–289.
[13] C.L. Bottasso, O.A. Bauchau, J.-Y. Choi, An energy decaying scheme for nonlinear dynamics of shells, Comput. Methods Appl. Mech. Engrg. 191 (2002) 3099–3121.
[14] C.L. Bottasso, M. Borri, L. Trainelli, Integration of elastic multibody systems by invariant conserving/dissipating algorithms. II. Numerical schemes and applications, Comput. Methods Appl. Mech. Engrg. 190 (2001) 3701–3733.
[15] B. Brank, L. Briseghella, N. Tonello, F.B. Damjanic, On non-linear dynamics of shells: implementation of energy–momentum conserving algorithm for a finite rotation shell model, Int. J. Numer. Methods Engrg. 42 (1998) 409–442.

[16] B. Brank, J. Korelc, A. Ibrahimbegović, Dynamics and time-stepping schemes for elastic shells undergoing finite rotations, Comput. Struct. 81 (12) (2003) 1193–1210.
[17] N. Büchter, E. Ramm, Shell theory versus degeneration – a comparison in large rotation finite element analysis, Int. J. Numer. Methods Engrg. 34 (1992) 39–59.
[18] E.N. Dvorkin, K.-J. Bathe, A continuum mechanics based four-node shell element for general nonlinear analysis, Engrg. Comput. 1 (1984) 77–88.
[19] C.W. Gear, G.K. Gupta, B.J. Leimkuhler, Automatic integration of the Euler–Lagrange equations with constraints, J. Comput. Appl. Math. 12 (1985) 77–90.
[20] M. Géradin, A. Cardona, Flexible Multibody Dynamics: A Finite Element Approach, John Wiley & Sons, 2001.
[21] O. Gonzalez, Time integration and discrete Hamiltonian systems, J. Nonlinear Sci. 6 (1996) 449–467.
[22] O. Gonzalez, Mechanical systems subject to holonomic constraints: differential-algebraic formulations and conservative integration, Physica D 132 (1999) 165–174.
[23] B. Göttlicher, K. Schweizerhof, Analysis of flexible structures with occasionally rigid parts under transient loading, Comput. Struct. 83 (2005) 2035–2051.
[24] T.J.R. Hughes, The Finite Element Method, Prentice-Hall, New Jersey, 1987.
[25] T.J.R. Hughes, W.K. Liu, Nonlinear finite element analysis of shells: Part I. Three-dimensional shells, Comput. Methods Appl. Mech. Engrg. 26 (1981) 331–362.
[26] A. Ibrahimbegović, S. Mamouri, R.L. Taylor, A.J. Chen, Finite element method in dynamics of flexible multibody systems: modeling of holonomic constraints and energy conserving integration schemes, Multibody Syst. Dyn. 4 (2-3) (2000) 195–223.
[27] G. Jelenić, M.A. Crisfield, Dynamic analysis of 3D beams with joints in presence of large rotations, Comput. Methods Appl. Mech. Engrg. 190 (2001) 4195–4230.
[28] L. Vu-Quoc, H. Deng, X.G. Tan, Geometrically-exact sandwich shells: the dynamic case, Comput. Methods Appl. Mech. Engrg. 190 (22–23) (2001) 2825–2873.
[29] S. Leyendecker, P. Betsch, P. Steinmann, Objective energy–momentum conserving integration for the constrained dynamics of geometrically exact beams, Comput. Methods Appl. Mech. Engrg. 195 (2006) 2313–2333.
[30] S. Leyendecker, P. Betsch, P. Steinmann, The discrete null space method for the energy consistent integration of constrained mechanical systems. Part III: Flexible multibody dynamics, Multibody Syst. Dyn. 19 (1–2) (2008) 45–72.
[31] I. Lubowiecka, J. Chróścielewski, On dynamics of flexible branched shell structures undergoing large overall motion using finite elements, Comput. Struct. 80 (2002).
[32] J.E. Marsden, T.S. Ratiu, Introduction to Mechanics and Symmetry, second ed., Springer-Verlag, 1999.
[33] J. Muñoz, G. Jelenić, Sliding joints in 3D beams: conserving algorithms using the master-slave approach, Multibody Syst. Dyn. 16 (3) (2006) 237–261.
[34] M.A. Puso, An energy and momentum conserving method for rigid-flexible body dynamics, Int. J. Numer. Methods Engrg. 53 (2002) 1393–1414.
[35] I. Romero, F. Armero, Numerical integration of the stiff dynamics of geometrically exact shells: an energy-dissipative momentum-conserving scheme, Int. J. Numer. Methods Engrg. 54 (2002) 1043–1086.
[36] J.C. Simo, On a stress resultant geometrically exact shell model. Part VII: Shell intersections with 5/6-DOF finite element formulations, Comput. Methods Appl. Mech. Engrg. 108 (1993) 319–339.
[37] J.C. Simo, D.D. Fox, On a stress resultant geometrically exact shell model. Part I: Formulation and optimal parametrization, Comput. Methods Appl. Mech. Engrg. 72 (1989) 267–304.
[38] J.C. Simo, M.S. Rifai, D.D. Fox, On a stress resultant geometrically exact shell model. Part VI: Conserving algorithms for non-linear dynamics, Int. J. Numer. Methods Engrg. 34 (1992) 117–164.
[39] J.C. Simo, N. Tarnow, A new energy and momentum conserving algorithm for the nonlinear dynamics of shells, Int. J. Numer. Methods Engrg. 37 (1994) 2527–2549.
[40] J.C. Simo, N. Tarnow, K.K. Wong, Exact energy–momentum conserving algorithms and symplectic schemes for nonlinear dynamics, Comput. Methods Appl. Mech. Engrg. 100 (1992) 63–116.
[41] G.M. Stanley, K.C. Park, T.J.R. Hughes, Continuum-Based Resultant Shell Elements, Finite Element Methods for Plate and Shell Structures, Pineridge Press, Swansea, 1986.
[42] R.L. Taylor, Finite element analysis of rigid-flexible systems, in: J.A.C. Ambrósio, M. Kleiber (Eds.), Computational Aspects of Nonlinear Structural Systems with Large Rigid Body Motion of NATO Science Series: Computer & Systems Sciences, vol. 179, IOS Press, 2001, pp. 63–84.